

# The Physics of Heavy Quark Distributions in Hadrons: Collider Tests

S.J. Brodsky<sup>a</sup>, V.A. Bednyakov<sup>b</sup>, G.I. Lykasov<sup>b,\*</sup>, J. Smiesko<sup>c</sup>, S. Tokar<sup>c</sup>

<sup>a</sup>*SLAC National Accelerator Laboratory, Stanford University, Menlo Park, CA 94025, United States*

<sup>b</sup>*Joint Institute for Nuclear Research, Dubna 141980, Moscow region, Russia*

<sup>c</sup>*Comenius University in Bratislava, Faculty of Mathematics, Physics and Informatics, Mlynska Dolina, 842 48 Bratislava, Slovakia*

---

## Abstract

We present a review of the current understanding of the heavy quark distributions in the nucleon and their impact on collider physics. The origin of strange, charm and bottom quark pairs at high light-front (LF) momentum fractions in hadron wavefunctions — the “intrinsic” quarks, is reviewed. The determination of heavy-quark parton distribution functions (PDFs) is particularly significant for the analysis of hard processes at LHC energies. We show that a careful study of the inclusive production of open charm and the production of  $\gamma/Z/W$  particles, accompanied by the heavy jets at large transverse momenta can give essential information on the intrinsic heavy quark (IQ) distributions. We also focus on the theoretical predictions concerning other observables which are very sensitive to the intrinsic charm contribution to PDFs including Higgs production at high  $x_F$  and novel fixed target measurements which can be tested at the LHC.

*Keywords:* Quarks, gluons, charm, QCD, PDF.

---



---

\*Corresponding author

*Email address:* lykasov@jinr.ru (G.I. Lykasov)

## Contents

<b>1</b>	<b>Introduction</b>	<b>3</b>
1.1	Motivation of this review . . . . .	3
1.2	Outline of this Review . . . . .	8
<b>2</b>	<b>Extrinsic and intrinsic quark components in nucleon</b>	<b>8</b>
2.1	Intrinsic charm density in a proton as a function of IC probability $w$	16
<b>3</b>	<b>Intrinsic heavy quarks and hard <math>pp</math> collisions</b>	<b>20</b>
3.1	Where can one look for the intrinsic heavy quarks? . . . . .	20
<b>4</b>	<b>Intrinsic strangeness in proton</b>	<b>23</b>
<b>5</b>	<b>Global analysis of PDFs with intrinsic charm</b>	<b>25</b>
<b>6</b>	<b>Intrinsic heavy quark signal in processes at collider energies</b>	<b>27</b>
6.1	Inclusive production of charmed meson . . . . .	27
6.2	Inclusive production of Higgs boson and intrinsic charm and bottom in proton . . . . .	29
6.3	Production of prompt photon and $c$ or $b$ -jet in hard $pp$ collisions	31
6.4	Production of $\gamma(Z) + c(b)$ -jet within the $k_T$ -factorization and the MCFM . . . . .	35
6.5	Prompt photon and open charm production . . . . .	48
6.6	$W(Z)$ -boson and $b(c)$ -jet production . . . . .	48
<b>7</b>	<b>Conclusion</b>	<b>62</b>
<b>8</b>	<b>Acknowledgements</b>	<b>64</b>
<b>9</b>	<b>References</b>	<b>65</b>

## 1. Introduction

### 1.1. Motivation of this review

The knowledge of the heavy quark distributions of the proton can provide fundamental information on nucleon structure. Since many hard processes within the Standard Model (SM) and beyond, such as the production of heavy jets and Higgs boson production, etc., are sensitive to the heavy quark content of the nucleon, heavy quark distributions play an increasingly significant role in the physics program of the Large Hadron Collider (LHC). The parton distribution functions (PDFs) of the strange, charm, and bottom quarks and their evolution are essential inputs for the calculation of these processes within perturbative quantum chromodynamics (pQCD). The heavy quark PDFs reflect both the initial conditions at momentum transfers below a factorization scale  $Q^2 < Q_0^2$  as dictated by the non-perturbative QCD color-confining dynamics of the proton plus the effects of pQCD which generates heavy quarks from the evolution of the light quark and gluon PDFs. A global QCD analysis allows one to extract the PDFs from the comparison of hard-scattering data based on the factorization properties of QCD.

In fact, QCD predicts two separate and distinct contributions to the heavy quark distributions  $q(x, Q^2)$  of the nucleons at low and high  $x$ . Here  $x = \frac{k^+}{P^+} = \frac{k^0 + k^3}{P^0 + P^3}$  is the frame-independent light-front (LF) momentum fraction carried by the heavy quark in a hadron with momentum  $P^\mu$ . In the case of deep inelastic lepton-proton scattering, the LF momentum fraction variable  $x$  in the proton structure functions can be identified with the Bjorken variable  $x_{\text{Bj}} = \frac{Q^2}{2p \cdot q}$ . At small  $x$ , heavy-quark pairs are dominantly produced via gluon-splitting subprocess  $g \rightarrow Q\bar{Q}$ . The existence of the heavy quarks in the nucleon from this standard contribution is a result of the QCD evolution of the light quark and gluon PDFs. The gluon splitting contribution to the heavy-quark degrees of freedom are perturbatively calculable using the Dokshitzer-Gribov-Lipatov-Altarelli-Parisi (DGLAP) evolution equation [1–3]. To first approximation, the heavy quark distribution falls as  $(1 - x)$  times the gluon distribution.

However, the QCD also predicts additional Fock state contributions to the proton structure at high  $x$ , such as  $|uudQ\bar{Q}\rangle$ , where the heavy quark pair is multiply connected to two or more valence quarks of the proton. This contribution depends on non-perturbative distribution of valence quarks in the hadron, and is maximal at minimal off-shellness; i.e., when the constituents all have the same rapidity  $y_i$  and thus  $x_i \propto \sqrt{m_i^2 + \vec{k}_{Ti}^2}$ . The heavy quark contributions to the nucleon's PDF thus peak at large  $x$ . Since they depend on the correlations determined by the valence quark distributions, these heavy quark contributions are *intrinsic* contributions to the hadron's fundamental structure. Furthermore, since all of the intrinsic quarks in the  $|uudQ\bar{Q}\rangle$  Fock state have similar rapidities they can reinteract, leading to significant  $Q$  vs.  $\bar{Q}$  asymmetries. In contrast, the contribution to the heavy quark PDFs arising from gluon splitting are symmetric in  $Q$  vs.  $\bar{Q}$ . Since they only depend on the gluon distribution, the contributions generated by DGLAP evolution can be considered as *extrinsic* contributions.

The PDFs at a fundamental level are computed from the squares of the hadrons' light-front wavefunctions, the frame-independent eigensolutions of the QCD Light-Front Hamiltonian. The intrinsic contributions are associated with amplitudes such as  $gg \rightarrow Q\bar{Q} \rightarrow gg$  in the self-energy of the proton, the analogs of light-by-light scattering  $\gamma\gamma \rightarrow \ell\bar{\ell} \rightarrow \gamma\gamma$  in QED, i.e., twist-6 contributions proportional to the gluon field strength of the order 3 in the operator product expansion (OPE). Thus the OPE provides a first-principle derivation for the existence of intrinsic heavy quarks.

Unlike the conventional  $\log m_Q^2$  dependence of the low  $x$  extrinsic gluon-splitting contribution, the probabilities for the intrinsic heavy quark Fock states at high  $x$  scale as  $\frac{1}{m_Q^2}$  in non-Abelian QCD. In contrast the probability for a higher Fock state in an atom such as  $|e^+e^-\ell\bar{\ell}\rangle$  in positronium scales as  $\frac{1}{m_\ell^4}$  in Abelian QED, corresponding to the twist-8 Euler-Heisenberg light-by-light insertion. Detailed derivations based on the OPE have been given in [4, 5].

When a proton collides with another proton or nucleus, the off-shell intrinsic heavy quark Fock state fluctuations such as  $|uudc\bar{c}\rangle$  are materialized and can produce open or hidden charm states at high momentum fraction. For example,

the comoving  $udc$  quarks in a Fock state such as  $|uudc\bar{c}\rangle$  can coalesce to produce a  $\Lambda_c(udc)$  baryon with a high Feynman momentum fraction  $x_F = x_c + x_u + x_d$  or produce a  $J/\psi$  with  $x_F = c\bar{c}$ . Such high  $x_F$  heavy hadron events have been observed and measured with substantial cross sections at the ISR proton-proton collider at fixed target experiments such as NA3 at CERN and SELEX at FermiLab. The  $\Lambda_b(udb)$  baryon was first observed at the ISR in forward  $pp \rightarrow \Lambda_b X$  reactions at high  $x_F$ .

The hypothesis of the *intrinsic* quark components in the proton was suggested in [6] to explain the large cross-section for the forward open charm production in  $pp$  collision at ISR energies [7–10]. The magnitude of the ISR cross sections suggests that the intrinsic charm probability in the proton is approximately of order 1 %; however, theoretical and experimental uncertainties make it difficult to make an accurate estimate.

Intrinsic charm is also important for charm production in cosmic ray experiments that measure charm production from high energy experiments interacting in the earth’s atmosphere. It also is important for estimating the high energy flux of neutrinos observed in the IceCube experiment. In fact one finds [11] that the prompt neutrino flux arising from charm hadroproduction by protons interacting in the earth’s atmosphere which is due to intrinsic charm is comparable to the extrinsic contribution if one normalizes the intrinsic charm differential cross sections to the ISR and the LEBC-MPS collaboration data.

Most measurements of  $c$  and  $b$ -jet production in deep inelastic lepton-proton scattering are consistent with the extrinsic gluon-splitting perturbative origin of heavy flavor quarks [12] alone. However, these experiments are not sensitive to the heavy quark distributions at large  $x$  region, where the theory predicts a non zero contribution of the so called *intrinsic* heavy-quark components in the proton wave function [4, 6, 13], as is suggested in Refs. [14–16].

The first direct experimental indication for the *intrinsic* heavy quarks in a nucleon was observed at the EMC measurement of the charm structure function at large  $x$  [17]. The measurement of the charm structure function at high  $x_{Bj}$  by the EMC experiment at CERN using deep inelastic muon-nucleus scatter-

ing showed a significant contribution to the proton structure function at large  $x_{\text{Bj}}$  [17]. In fact, the charm structure function  $c(x, Q)$  measured by the EMC collaboration was approximately 30 times higher than expected from gluon splitting and at  $x_{\text{Bj}} = 0.42$  and  $Q^2 = 75 \text{ (GeV/c)}^2$ . As shown in Refs. [18–20], the inclusion of both the HERA data and the EMC data to the global NNPDF analysis allows one to do a model independent determination of the charm content of the proton. The results of Ref. [18] suggest the perturbative origin of the charm PDF at  $x < 0.1$ , which vanishes at  $\mu \simeq 1.5 \text{ GeV/c}$ , but it also indicate presence of a large  $x$  *intrinsic* component picked at  $x \sim 0.5$  and carried  $0.7 \pm 0.3 \%$  of the nucleon momentum with the 68 % CL at low scale  $\mu_0 = 1.65 \text{ GeV/c}$ .

There have been attempts to describe the data [21–23] on inclusive spectra of the open charm production in soft  $pp$  collisions and the asymmetry between the  $D^-$  and  $D^+$  production in  $\pi^-p$  collisions within the string model [24, 25] without the assumption on the *intrinsic* charm in a nucleon. However, the description of data is very sensitive to the fragmentation functions of  $c$ -quarks to charmed hadrons, the knowledge of which up to now is not sufficient, see, e.g. Refs. [26–28]. Moreover, the experimental data on the open charm production, for example,  $\Lambda_c^+$  in  $pp$  collision at the ISR energies and large  $x$ , have large uncertainty [29, 30].

The existence of the *intrinsic* heavy quark components can be observed not only in the forward kinematic region, but also in hard  $pp$  processes of photon or vector boson production in association with the heavy flavor jets. The first hint on this was observed at the Tevatron ( $\sqrt{s} = 1.96 \text{ TeV}$ ) in the production of prompt photons accompanied by heavy jets ( $c$  or  $b$ ) [31–35]. The basic underlying hard subprocesses are  $gc \rightarrow \gamma c$  and  $gb \rightarrow \gamma b$ . The measurements of  $pp \rightarrow b\gamma X$  at high  $p_T$  are consistent with standard analyses where the  $b$  quark PDF arises from gluon splitting  $g \rightarrow b\bar{b}$ . However, the  $pp \rightarrow c\gamma X$  data show a significant excess, indicating that the charm PDF has significant support at large  $x$ . This is consistent with the fact that the ratio of intrinsic bottom to charm probabilities in the proton scales as  $m_c^2/m_b^2$  [36].

It was observed that the ratio between the experimental spectrum of the

prompt photon accompanied by the  $c$ -jets and the theoretical calculation, which used the PDF without the IC, increases with  $p_T^\gamma$  up to factor of about 3 at  $p_T^\gamma \simeq 110$  GeV/ $c$ . The inclusion of the IC contribution obtained within the BHPS model [6, 13] allows one to reduce this ratio up to 1.5 [37]. This stimulated us to investigate the hard processes of the production of prompt photons or gauge vector bosons accompanied by heavy flavor jets ( $c$  or  $b$ ) in  $pp$  collisions at the LHC energies [38, 39]. It was shown that at large transverse momenta of  $\gamma$  or  $Z/W$  ( $p_T > 100$  GeV/ $c$ ) and their rapidities  $y > 1.5$  the *intrinsic* charm can contribute to the  $p_T$ -spectra of these particles. Therefore, these processes can be used as a laboratory to search for the IC contribution. It was shown [40] that a possible observation of the IC contribution looks very promising at the LHC in processes like  $pp \rightarrow \gamma/Z/W + c/b + X$ . The main goal of this review is to show, how the *intrinsic* heavy quark components in a nucleon can be tested at the LHC.

In addition to the processes discussed above the more exotic observables, for example, the diffractive and inclusive Higgs boson production in  $pp$  collisions at LHC energies can give an information on the non-zero contribution of the *intrinsic* heavy flavor components to the proton PDF [41, 42]. In the  $x_F$ -distribution of the diffractive Higgs boson production in  $pp$  collision a peak is predicted at  $x_F \sim 0.9$ , which is due to the *intrinsic charm* (IC) contribution [41]. In [42] a similar enhancement in the  $x_F$ -spectrum of the inclusive Higgs boson production is predicted at  $x_F \sim 0.8 - 0.9$  due to the *intrinsic bottom* (IB) contribution to the proton PDF. Recently a proposal to observe the IC signal at the high luminosity fixed-target experiment using the LHC beam (AFTER@LHC) [43] was suggested, see review [15] and references therein. All these predictions concern mainly the forward production of heavy hadrons at large longitudinal fraction of their momentum  $x_F > 0.5$ , therefore, in principle, the *intrinsic* heavy quark signal in such observables could be visible. However, a high experimental accuracy is needed to observe the enhancement in the heavy hadron spectra due to the IC or IB contribution to the proton PDF.

## 1.2. Outline of this Review

The review consists of 7 sections. In Section 2 we present a more detailed overview of the concepts of extrinsic and intrinsic quark components in a nucleon and their distinction. In Section 3 we show why the *intrinsic* quark components can be visible in the hard  $pp$  processes at high energies. Section 4 is devoted to the *intrinsic strangeness* (IS) content of the nucleon and search for it in hard  $pp$  collisions at high energies. Section 5 is a short overview of the global analysis of PDFs with intrinsic charm. Section 6 is devoted to search for the *intrinsic* heavy quark in processes at collider energies, namely, in the inclusive production of open charm or Higgs boson and production of prompt photons  $\gamma$  or gauge vector bosons  $W/Z$  accompanied by  $c(b)$ -jets or open charm in  $pp$  collision at LHC energies. There we discuss a possible test of the IC contribution in proton at LHC. Finally, in Section 7 we present the conclusion.

## 2. Extrinsic and intrinsic quark components in nucleon

By definition, the PDF  $f_a(x, \mu)$  is a function of the proton momentum fraction  $x$  carried by parton  $a$  (quark  $q$  or gluon  $g$ ) at the QCD momentum transfer scale  $\mu$ . For small values of  $\mu$ , corresponding to the long distance scales greater than  $1/\mu_0$ , the PDF cannot be calculated from the first principles of QCD (although some progress in this direction has been recently achieved within the lattice methods [44, 45]). If the PDF  $f_a(x, \mu)$ , is known at a scale  $\mu > \mu_0$ , one can calculate it at any other scale  $\mu$  by solving the perturbative QCD evolution equations (DGLAP) [1–3]; usually, the value of the starting scale  $\mu_0$  is chosen about a few GeV/ $c$ . As the input of evolution functions  $f_a(x, \mu_0)$  can be taken at any scale the functions can be found empirically from some “QCD global analysis” [46–48] of a large variety of data, typically at  $\mu > \mu_0$ .

In general, almost all  $pp$  processes that took place at the LHC energies, including the Higgs boson production, are sensitive to the charm  $f_c(x, \mu)$  or bottom  $f_b(x, \mu)$  PDFs. Heavy quark become visible in proton at scales  $\mu_c$  and  $\mu_b$  and their contents increases with increasing  $Q^2$ -scale through the gluon splitting

in the DGLAP  $Q^2$  evolution [1–3]. Direct measurement of the open charm and open bottom production in the deep inelastic processes (DIS) confirms the QCD picture of heavy quarks dynamics in proton [12].

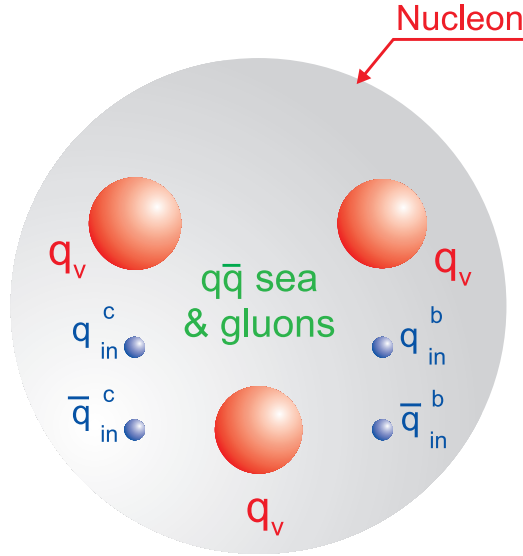


Figure 1: Schematic presentation of a proton during the  $pp$  collision during the  $pp$  collision at a value of  $Q^2$ , when the lifetime of the *intrinsic* Fock-state is much larger than the interaction time.

As was assumed in [6, 13], there are *extrinsic* and *intrinsic* contributions to the quark-gluon structure of the proton. The *extrinsic* (or perturbative sea) quarks and gluons are generated on a short time scale associated with a large transverse momentum processes as a result of gluon dynamics. Their distribution functions satisfy the standard QCD evolution equations [1–3]. The *extrinsic* quark contribution  $q_{\text{ex}}(x)$  to PDFs is mostly significant at low  $x$  and decreases when the quark momentum fraction grows. It depends logarithmically on the heavy quark mass  $M_Q$ , while the *intrinsic* quark contribution  $q_{\text{in}}(x)$ , the residual part of the proton structure not coming from the perturbative gluon splitting, is almost zero at low  $x$  and dominates compared to the *extrinsic* one at large  $x > 0.1$ . It depends on the heavy quark mass as  $1/M_Q^2$ . Initially in [6, 13] authors have proposed existence of the 5-quark state in a proton, which con-

sists of valence  $uud$  quarks and the charm-anticharm pair  $c\bar{c}$ , i.e.,  $|uudc\bar{c}\rangle$ . This model is called as the BHPS model, in the frame of which it was assumed that  $c(x) = \bar{c}(x)$ . Later it was shown within the light-cone meson-baryon fluctuation model [49] that the *intrinsic* quarks and antiquarks cannot be identical in contrast to the *extrinsic* quarks and antiquarks, which are necessarily CP symmetric because they are produced from the gluon splitting. The distributions of  $q_{\text{ex}}(x)$  in comparison with  $q_{\text{in}}(x)$  exhibits a series of distinctions [6, 13, 15] explained in the following. The *extrinsic* heavy quarks are generated by gluon splitting, therefore their PDFs are softer than those of the parent gluon by a factor of  $(1-x)$ . In contrast, the *intrinsic* heavy quark state in proton  $|uudq_{\text{in}}\bar{q}_{\text{in}}\rangle$  is dominated at high  $x$ , when it is minimally off shell and the *intrinsic* quarks distributions correspond to those of constituent quarks. The resulting momentum and spin distributions of *intrinsic*  $q_{\text{in}}$  and  $\bar{q}_{\text{in}}$  can be  $q_{\text{in}}(x) \neq \bar{q}_{\text{in}}(x)$ . One can argue that the proton quantum numbers are identical with those of  $uud$  and so the intrinsic PDFs of  $q_{\text{in}}$  and  $\bar{q}_{\text{in}}$  should be identical but with opposite spins. Fig. 1 shows a schematic view of a nucleon, which consists of three valence quarks  $q_v$ , the quark-antiquark pairs can be created by a diagram similar to the cut self-energy graph within the QED. In principle, these pairs can be both the light quark-antiquark pair  $q\bar{q}$  and heavy quark-antiquark  $Q\bar{Q}$  pair. However, the distribution of the *intrinsic* heavy quark  $Q\bar{Q}$  components dominates compared to the *intrinsic* light  $q\bar{q}$  components at large  $x > 0.1$ , as will be discussed later, see also [15, 50]. Therefore, we will focus mainly on the properties of heavy flavor *intrinsic*  $Q\bar{Q}$  pairs in a nucleon.

According to Fig. 2, if the gluon-gluon scattering box diagram,  $gg \rightarrow Q\bar{Q} \rightarrow gg$ , is inserted into the proton self-energy graph, the cut of this amplitude generates five-quark Fock states of the proton  $|uudQ\bar{Q}\rangle$  [15].

It was shown in [13] that the existence of *intrinsic* heavy quark pairs  $c\bar{c}$  and  $b\bar{b}$  within the proton state could be due to the diagrams where heavy quarks are multiply connected to valence quarks. On this basis, within the MIT bag model [51], the probability to find the five-quark component  $|uudc\bar{c}\rangle$  bound within the nucleon bag was estimated to be about 1 – 2 %. Later some other

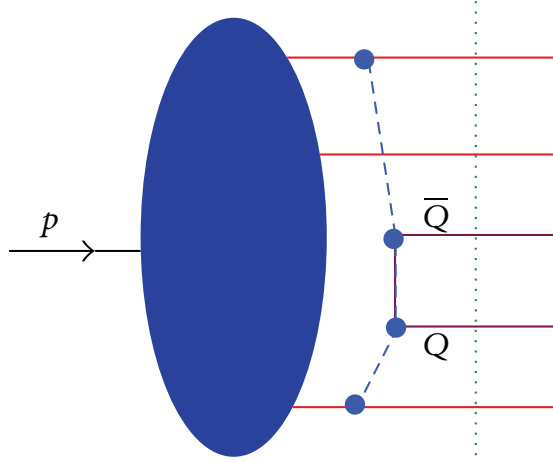


Figure 2: Schematic graph of the  $Q\bar{Q}$  pair creation in a nucleon.

models were also developed [16, 50, 52–55]. One of them considered a quasi-two-body state  $\bar{D}^0(u\bar{c})\bar{\Lambda}_c^+(udc)$  in the proton [16]. In [16, 50, 56] the probability to find the intrinsic charm (IC) in the proton (the weight of the relevant Fock state in the proton) was assumed to be 1 – 3.5 %. The probability of the intrinsic bottom (IB) in the proton is suppressed by the factor  $m_c^2/m_b^2 \simeq 0.1$  [36], where  $m_c$  and  $m_b$  are the masses of the charmed and bottom quarks.

The probability distribution for the 5-quark state ( $|uudc\bar{c}\rangle$ ) in the light-cone description of the proton was first calculated in [6]. The general form for this distribution calculated within the light-cone dynamics in the so-called BHPS model [6, 13] can be written as [16]

$$dP = N \prod_{j=1}^5 \frac{dx_j}{x_j} \delta\left(1 - \sum_{j=1}^5 x_j\right) \prod_{j=1}^5 d^2p_{Tj} \delta^{(2)}\left(\sum_{j=1}^5 p_{Tj}\right) \frac{F^2(s)}{(s - m_N^2)^2}, \quad (1)$$

where

$$s = \sum_{j=1}^5 \frac{p_{Tj}^2 + m_j^2}{x_j} \quad (2)$$

and  $x_j$  is the longitudinal momentum fraction of the parton,  $m_j$  is its mass and  $m_N$  is the nucleon mass. The form factor  $F^2$  characterizes the dynamics of the bound state. It suppresses the contributions at large values of  $p_{Tj}$  and small  $x_j$

to make the integrated probability  $P$  converge.

LFWFs (light front wave functions) are defined at a fixed LF (light front) time  $\tau = t + z/c$ . They are arbitrarily off-shell in  $P^- = P^0 - P^3$  and thus invariant mass  $W$ .

The intrinsic heavy quark LF Fock states such as  $|uudQ\bar{Q}\rangle$  arise from standard QCD — any diagram where the  $Q\bar{Q}$  is multi-connected to the valence Fock states.

The simplest IQ Fock states correspond to the insertion of gluon-gluon scattering  $gg \rightarrow Q\bar{Q} \rightarrow gg$  in the hadron self-energy. Its cut diagram is presented in Fig. 2.

The LFWFs are maximal at minimal off-shellness; i.e., minimum invariant mass. This occurs when all of the constituents have the same rapidity and thus  $x_i \propto \sqrt{m_i^2 + k_{T,i}^2}$ . This is why the heavy partons have the highest LF  $x_i$ .

Even in QED one has intrinsic heavy lepton states such as  $|e^+e^-\mu^+\mu^-\rangle$  LF Fock states. In the Abelian case the intrinsic heavy lepton probability falls as  $\frac{1}{\mathcal{M}^4}$ , where  $\mathcal{M}$  is the effective mass of this system. In contrast, the probability falls as  $\frac{1}{\mathcal{M}^2}$  in non-Abelian QCD. Thus one has a direct way to validate QCD.

One could actually measure the  $x$  of distributions of such Fock states in positronium by colliding and dissociating relativistic positronium atoms in a gas jet target:  $[e^+e^-]Z \rightarrow e^+e^-\mu^+\mu^-Z$ .

This is the analog of the Ashery experiment  $\pi A \rightarrow q\bar{q}A$  which measured the LFWF of the pion.

Since the quarks in  $|uudQ\bar{A}\rangle$  tend to have the same rapidity, they will continue to reinteract. This causes the  $s(x)\bar{s}(x)$  asymmetry in the proton PDF.

IQ is rigorous — it is a first-principle prediction of QCD. It can be analysed using the OPE as shown by M. Polyakov et al. [36] and earlier by paper from S.J. Brodsky et al. [4].

The production cross-section for  $\gamma^*p \rightarrow c\bar{c}$  vanishes as a power of  $W^2 - W_{\text{threshold}}^2$ . This is why one cannot reliably use SLAC data to test IC, as noted by Gardner and Brodsky. Very few events satisfy this cut [57].

The IQ states will be produced at small rapidity  $\Delta y$  relative to the SMOG

nuclear target in the LHCb fixed target experiment [58]. This provides an amazing testing ground for IQ.

One can thus validate the ISR experiments which measured  $\Lambda_c$  and  $\Lambda_b$  at high  $x_F$  [29, 30]. This leading particle phenomena was also observed by SELEX [59] in  $pA \rightarrow \Lambda_c X$ .

A dramatic consequence of IQ: Higgs boson production at high  $x_F > 0.8$  at the ISR. This is supported by the measurement of  $J/\psi$  by Badier et al. (NA3) and even double  $J/\psi$  hadroproduction at high  $x_F$  [41, 42, 60].

Neglecting all the quark masses in comparison with the nucleon mass and the charm quark mass  $m_c$ , and integrating (1) over  $dx_1 \dots dx_4$  and putting  $F^2 = 1$  in Eq. (1) one can get the following probability to find the intrinsic charm with momentum fraction  $x \equiv x_5$  in the nucleon [61]

$$P(x) = \frac{Nx^2}{6(1-cx)^5} \left( \phi_1(x) + \phi_2(x) [\ln(x) - \ln[1-c(1-x)x]] \right), \quad (3)$$

where  $x = x_5$ ,  $c = m_N^2/m_c^2$ ,

$$\phi_1(x) = (1-x)(1-cx) \left[ 1 + x \left[ 10 + x - c(1-x) \left( x(10 - c(1-x)) + 2 \right) \right] \right], \quad (4)$$

and

$$\phi_2(x) = 6x [1 + x(1 - c(1-x))] [1 - c(1-x)x]. \quad (5)$$

Here  $N$  is found from the normalization equation:

$$\int_0^1 P(x) dx = w, \quad (6)$$

where  $w$  is the integral fraction of the intrinsic charm. Setting  $c \rightarrow 0$  leads to the BHPS result [6, 16, 61]:

$$P(x) = 600wx^2 \left[ 6x(1+x) \ln x + (1-x)(1+10x+x^2) \right], \quad (7)$$

Equation (7) was first derived by Brodsky, Hoyer, Peterson and Sakai [6] and, usually, this approach is called as the BHPS model. In principle, the form factor  $F^2$  can be less than 1. It is due to the suppression of the high mass configurations

in Eq. (7). For example, it can be chosen as the *exponential suppression* factor [16]:

$$F^2 = \exp\left(\frac{-(s - m_{\text{N}}^2)}{\Lambda^2}\right). \quad (8)$$

or the *power-low suppression* factor:

$$F^2 = \frac{1}{(s + \Lambda^2)^n}. \quad (9)$$

As is shown in [16], the results for  $P(x)$  using the exponential or power-low suppression factor with  $n = 4$  are rather similar to the BHPS model, but are somewhat smaller at  $x > 0.5$ . Values  $n \leq 2$  are unphysical because they result in the total probability divergence [16] and the use Eq. (9) at  $n = 3$  leads to a dependence  $F^2 \sim 1/m_c^2$  that is similar to the result of [5].

Another way to suppress the high-mass Fock space components can be made on the basis of quasi-two-body states [16, 49]. In particular, the relevant 5-quark Fock configurations can be grouped as  $(udc)(u\bar{c})$  considered as the off-shell two-body state  $\bar{D}^0\Lambda_c^+$ . In this case the factor  $F^2$  is chosen, for example, in [16] as power-low suppression and can be different for  $\bar{D}^0$  and  $\Lambda_c^+$ . It leads to the asymmetry between the  $c$  and  $\bar{c}$ -distribution, which was considered first in [49]. The observation of a  $c(x) - \bar{c}(x)$  difference can definitively prove a non-perturbative charm quark component since the  $c\bar{c}$  pairs produced by gluon splitting are symmetric, according to the NLO calculations, whereas the NNLO calculations can give different shapes for  $c(x)$  and  $\bar{c}(x)$ , see for example, [16] and [62]. The charm and anti-charm distributions obtained within the cloud-model and can be parametrized by the following form at  $\mu^2 = m_c^2$  [50]:

$$c(x) = Nx^{1.897}(1-x)^{6.095}; \quad \bar{c}(x) = \bar{N}x^{2.511}(1-x)^{4.929}, \quad (10)$$

where  $N/\bar{N}$  is determined by the quark number sum rule [50]:

$$\int_0^1 [c(x) - \bar{c}(x)] dx = 0, \quad (11)$$

and the normalization factor is related to the IC probability. In fact, the asymmetry between  $\bar{\Lambda}_c^-$  and  $\Lambda_c^+$  baryons was observed by the SELEX Collaboration [63] in  $\Sigma^-p$  collision at the beam momentum about 600 GeV/c. This

asymmetry was about 50 % at  $x_F \simeq 0.3$ . However, in  $\pi^-p$  and  $pp$  collisions the asymmetry was practically invisible because of the very poor statistics.

For the strange-antistrange pairs asymmetry similar to the charm-anticharm one was predicted in [49] and [54] within the light-cone five meson-baryon fluctuation model assuming hypothesis about the *intrinsic strangeness* in a nucleon. The difference between  $c(x)$  and  $\bar{c}(x)$  was studied, for example, in [49]. Later we will discuss a possible verification of this quark-antiquark asymmetry of the nucleon sea at the LHC.

Alternatively, the relevant 5-quark configurations can be grouped as  $(uud)(c\bar{c})$  or the off-shell proton and  $J/\Psi$ -meson [16]. However, this quark combination does not result in the  $c - \bar{c}$  asymmetry.

In contrast to the light-cone approach of heavy flavor Fock quark components in a nucleon, the alternative purely phenomenological scenario was suggested [50]. In this model the charm distribution in a nucleon is *sea like*, i.e., similar to that of the light-flavor sea quarks  $c(x) = \bar{c}(x) = \bar{d}(x) + \bar{u}(x)$  at  $\mu_0^2 = m_c^2$ .

The initial non-perturbative forms for  $c(x)$  and  $\bar{c}(x)$  at  $\mu_0$  specified above are usually used as inputs to the general-mass perturbative DGLAP evolution. The *global analysis* of distributions of the *extrinsic* and *intrinsic* heavy-flavor and light-flavor quark distributions and gluons was performed in [50] on basis of the BHPS, the meson-cloud model, *sea like* scenario and the PDF of type CTEQ6.5, which does not contain the IC contribution. Therefore, we will not redraw the figures from [50] and [16], but let us discuss the main properties of these parton distributions as a function of  $x$  at different values of scale  $\mu$ . The BHPS model for the  $x$  distribution for intrinsic heavy flavor quarks was derived within the light-cone approach. The derivation uses some additional simplifying approximations, which can be modified. The shape of the intrinsic quark distribution versus  $x$  is due to its dependence on the energy propagator  $1/(s - m_N^2)$  in Eq. (1). Using the DGLAP  $\mu^2$ -evolution for parton distributions it was shown that the intrinsic charm provides the dominant contribution to  $c(x)$  and  $\bar{c}(x)$  at any  $\mu$ , if the form of the IC distribution is given by the BHPS model

with the non-zero IC probability  $w$ . The comparison of the charm distribution to other flavor distributions presented, for example, in [50] showed that the inclusion of the IC contribution with  $w = 1$  and 3.5 % leads to an enhancement, which is larger than the values of light sea quark distributions ( $u_{\text{sea}} = \bar{u}_{\text{sea}}$ ,  $d_{\text{sea}} = \bar{d}_{\text{sea}}$ ,  $s_{\text{sea}} = \bar{s}_{\text{sea}}$ ) at  $x > 0.4$  at any QCD scale  $\mu$ . The intrinsic charm contribution  $c_{\text{in}}(x)$  dominates compared to the extrinsic one  $c_{\text{ex}}(x)$  at  $x > 0.1$ . The shape of the charm quark distribution  $c(x) = c_{\text{ex}}(x) + c_{\text{in}}(x)$  is similar to the valence quark distribution, but is smaller by a factor of about 10 in the whole region of  $0.003 < x < 1$  at low  $\mu$  and in the region of  $x > 0.1$  at large  $\mu$ . The results for the IC distribution using the BHPS model and the  $D_0\Lambda_c^+$  meson-cloud model are close [50]. The *sea like* scenario results in no any enhancement for the charm quark distribution at  $x > 0.1$ , as it is within the BHPS and the meson-cloud models. However, the *sea like* model gives for  $c(x)$  an excess about a factor of 1.5 – 2 compared to the  $c_{\text{ex}}(x)$  at  $0.003 < x < 0.1$  and low  $\mu$  and there is no excess at large  $\mu \geq 100$  GeV/c.

### 2.1. Intrinsic charm density in a proton as a function of IC probability $w$

According to [15, 64, 65], the intrinsic charm distribution at the starting scale  $\mu_0^2$  as a function of  $x$  can be presented in the following approximated form similar to Eq. 7:

$$c_{\text{int}}(x, \mu_0^2) = c_0 w x^2 \left[ (1-x)(1+10x+x^2) + 6x(1+x) \ln(x) \right], \quad (12)$$

where  $w$  is the probability to find the Fock state  $|uudc\bar{c}\rangle$  in the proton,  $c_0$  is the normalization constant and the masses of the light quarks and the nucleon are negligible compared to the charm quark mass. The inclusion of the non-zero nucleon mass leads to a more complicated analytic form [50, 61]. According to the BHPS model [6, 13], the charm density in a proton is the sum of the *extrinsic* and *intrinsic* charm densities,

$$xc(x, \mu_0^2) = xc_{\text{ext}}(x, \mu_0^2) + xc_{\text{int}}(x, \mu_0^2). \quad (13)$$

The *extrinsic*, or ordinary quarks and gluons are generated on a short-time scale associated with the large-transverse-momentum processes. Their distri-

bution functions satisfy the standard QCD evolution equations. Contrariwise, the *intrinsic* quarks and gluons can be associated with a bound-state hadron dynamics and one believes that they have a non-perturbative origin. It was argued [13] that existence of *intrinsic* heavy quark pairs  $c\bar{c}$  and  $b\bar{b}$  within the proton state can be due to the gluon-exchange and vacuum-polarization graphs presented in Fig. 2.

The charm density  $xc(x, \mu^2)$  at an arbitrary scale  $\mu^2$  is calculated using the Dokshitzer-Gribov-Lipatov-Altarelli-Parisi (DGLAP) equations [1–3]. Such calculations were done by the CTEQ [56] and CT14 groups [20] at some fixed values of the IC probability  $w$ . Namely, the CTEQ group used  $w = 1\%$  and  $w = 3.5\%$ , and CT14 used  $w = 1\%$  and  $w = 2\%$ . To calculate the charm density function  $xc(x, \mu^2)$  at any reasonable value of  $w$ , we use the following approximation Eq. (14). In the general case, there is some mixing between two parts of Eq. (13) during the DGLAP evolution. It can be seen from comparison of our calculations of charmed quark densities presented in Fig. 3, where this mixing was included within the CTEQ [56] set, and Fig. 2 of [64], when the mixing between two parts of the charm density was neglected. Our results on the total charm density  $xc(x, \mu^2)$  are in good agreement with the calculations of [64] at the whole kinematical region of  $x$  because at  $x < 0.1$  the IC contribution  $xc_{\text{int}}$  is much smaller than the *extrinsic* one  $xc_{\text{ext}}$ . However, such mixing is negligible [64], especially at large  $\mu^2$  and  $x$ . Therefore, one can apply the DGLAP evolution separately to the first part  $xc_{\text{ext}}(x, \mu_0^2)$  and the second part  $xc_{\text{int}}(x, \mu_0^2)$  of Eq. (13).

Taking into account that the IC probability  $w$  enters into Eq. (13) as a constant in front of the function dependent on  $x$  and  $\mu^2$ , one can suggest a simple relation at any  $w \leq w_{\text{max}}$ :

$$xc_{\text{int}}(x, \mu^2) = \frac{w}{w_{\text{max}}} xc_{\text{int}}(x, \mu^2) \Big|_{w=w_{\text{max}}} . \quad (14)$$

Actually, Eq. 14 is the linear interpolation between two charm densities at the scale  $\mu^2$ , obtained at  $w = w_{\text{max}}$  and  $w = 0$ . Later we adopt the charm distribution function from the CTEQ66M set [56]. We assume  $w_{\text{max}} = 3.5\%$

everywhere, which corresponds to the CTEQ66c1 set [56].

The charmed quark densities at different  $w$  and  $\mu^2$  are shown in Fig. 3.

Our results are in good agreement with the calculations [64] but are obtained in the more straightforward manner. Additionally, we performed the three-point interpolation of the charmed quark distributions (over  $w = 0$ ,  $w = 1$  % and  $w = 3.5$  %, which correspond to the CTEQ66M, CTEQ66c0 and CTEQ66c1 sets, respectively). These results differ from the ones based on (14) by no more than 0.5 %, thus giving us the confidence in our starting point. The comparison to CT14 with IC 1 % and 2 % was also performed and it is in very good agreement with results obtained using Eq. (14). We conclude that the sensitivity of resulting distributions to choice of intrinsic charm PDF (CTEQ66 or CT14) is very small.

Below we apply the charmed quark density obtained by (13) and (14) to calculate the total and differential cross-sections of associated prompt photon  $\gamma$  or  $Z$  boson and heavy flavor jet production,  $\gamma(Z) + Q$ , at the LHC conditions. The suggested procedure to calculate  $x c_{\text{int}}(x, \mu^2)$  at any  $w \leq w_{\text{max}}$  allows us to reduce significantly the time for the calculation of these observables.

As a rule, the gluons and sea quarks play the key role in hard processes of open charm hadroproduction. Simultaneously, due to the non-perturbative *intrinsic* heavy quark components one can expect some excess of these heavy quark PDFs over the ordinary sea quark PDFs at  $x > 0.1$ . Therefore the existence of this intrinsic charm component can lead to some enhancement in the inclusive spectra of open charm hadrons, in particular  $D$ -mesons, produced at the LHC in  $pp$ -collisions at large pseudo-rapidities  $\eta$  and large transverse momenta  $p_T$  [66]. Furthermore, as we know from [6, 13, 16, 50, 51, 56] photons produced in association with heavy quarks  $Q(\equiv c, b)$  in the final state of  $pp$ -collisions provide valuable information about the parton distributions in the proton [16, 31–34, 36, 38, 50, 53, 56, 66–74].

In this paper, having in mind these considerations we will first discuss where the above-mentioned heavy flavor Fock states in the proton could be searched for at the LHC energies. Following this we analyze in detail, and give predictions

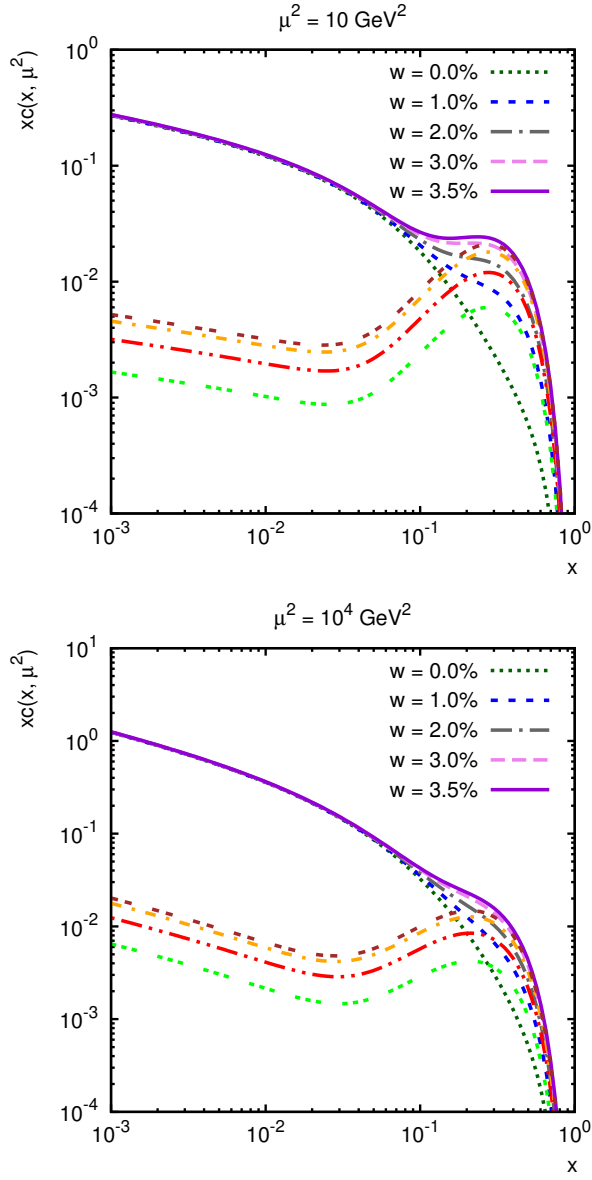


Figure 3: The total charmed quark density  $xc(x, \mu^2)$  as a function of  $x$  at different values of  $w$  at  $\mu^2 = 10 \text{ (GeV/c)}^2$  (top) and  $\mu^2 = 10^4 \text{ (GeV/c)}^2$  (bottom). The triple-dashed line is the IC contribution at  $w = 1 \%$ , the dashed-double-dotted line corresponds to the IC at  $w = 2 \%$ , the dashed-dotted curve is the IC at  $w = 3 \%$  and the double-dashed line corresponds to the IC at  $w = 3.5 \%$ .

for, the LHC semi-inclusive  $pp$ -production of prompt photons accompanied by  $c$ -jets including the *intrinsic* charm component in the PDF.

### 3. Intrinsic heavy quarks and hard $pp$ collisions

#### 3.1. Where can one look for the intrinsic heavy quarks?

It is known that in the open charm/bottom  $pp$ -production at large momentum transfer the hard QCD interactions of two sea quarks, two gluons and a gluon with a sea quark play the main role. The cross section for hard inclusive hadronic reactions  $pp \rightarrow hX$  can be factorized [75] as the product of structure and fragmentation functions convoluted with the sum of contributing  $2 \rightarrow 2$  quark and gluon subprocess  $i + j \rightarrow i' + j'$  cross sections. This result can be presented in the following general form [76] (see also [77]):

$$E \frac{d\sigma}{d^3p} = \sum_{i,j} \int d^2k_{Ti} \int d^2k_{Tj} \int_{x_i^{\min}}^1 dx_i \int_{x_j^{\min}}^1 dx_j f_i(x_i, k_{Ti}) f_j(x_j, k_{Tj}) \frac{d\sigma_{ij}(\hat{s}, \hat{t})}{d\hat{t}} \frac{D_{i,j}^h(z_h)}{\pi z_h}. \quad (15)$$

Here  $k_{i,j}$  and  $k'_{i,j}$  are the four-momenta of the partons  $i$  or  $j$  before and after the elastic parton-parton scattering, respectively;  $k_{Ti}$ ,  $k_{Tj}$  are the transverse momenta of the partons  $i$  and  $j$ ;  $z$  is the fraction of the hadron momentum from the parton momentum;  $f_{i,j}$  is the PDF; and  $D_{i,j}$  is the fragmentation function (FF) of the parton  $i$  or  $j$  into a hadron  $h$ .

When the transverse momenta of the partons are neglected in comparison with the longitudinal momenta, the variables  $\hat{s}$ ,  $\hat{t}$ ,  $\hat{u}$  and  $z_h$  can be presented in the following forms [75]:

$$\hat{s} = x_i x_j s, \quad \hat{t} = x_i \frac{t}{z_h}, \quad \hat{u} = x_j \frac{u}{z_h}, \quad z_h = \frac{x_1}{x_i} + \frac{x_2}{x_j}, \quad (16)$$

where

$$x_1 = -\frac{u}{s} = \frac{x_T}{2} \cot \frac{\theta}{2}, \quad x_2 = -\frac{t}{s} = \frac{x_T}{2} \tan \frac{\theta}{2}, \quad x_T = 2 \frac{\sqrt{tu}}{s} = 2 \frac{p_T}{\sqrt{s}}. \quad (17)$$

Here as usual,  $s = (p_1 + p_2)^2$ ,  $t = (p_1 - p'_1)^2$ ,  $u = (p_2 - p'_1)^2$ , and  $p_1$ ,  $p_2$ ,  $p'_1$  are the 4-momenta of the colliding protons and the produced hadron  $h$ , respectively;

$\theta$  is the scattering angle for the hadron  $h$  in the  $pp$  c.m.s. The lower limits of the integration in (15) are

$$x_i^{\min} = \frac{x_T \cot \frac{\theta}{2}}{2 - x_T \tan \frac{\theta}{2}}, \quad x_j^{\min} = \frac{x_i x_T \tan \frac{\theta}{2}}{2x_i - x_T \cot \frac{\theta}{2}}. \quad (18)$$

Actually, the parton distribution functions  $f_i(x_i, k_{iT})$  also depend on the four-momentum transfer squared  $Q^2$  that is related to the Mandelstam variables  $\hat{s}$ ,  $\hat{t}$ ,  $\hat{u}$  for the elastic parton-parton scattering [75, 76]

$$Q^2 = \frac{2\hat{s}\hat{t}\hat{u}}{\hat{s}^2 + \hat{t}^2 + \hat{u}^2} \quad (19)$$

One can see that the Feynman variable  $x_F$  of the produced hadron, can be expressed via the variables  $p_T$  and  $\eta$ , or  $\theta$  the hadron scattering angle in the  $pp$  c.m.s,

$$x_F \equiv \frac{2p_z}{\sqrt{s}} = \frac{2p_T}{\sqrt{s}} \frac{1}{\tan \theta} = \frac{2p_T}{\sqrt{s}} \sinh \eta. \quad (20)$$

At small scattering angles of the produced hadron this formula becomes

$$x_F \sim \frac{2p_T}{\sqrt{s}} \frac{1}{\theta}. \quad (21)$$

It is clear that for fixed  $p_T$  an outgoing hadron must possess a very small  $\theta$  or very large  $\eta$  in order to have large  $x_F$  (to follow forward, or backward direction).

In the fragmentation region (of large  $x_F$ ) the Feynman variable  $x_F$  of the produced hadron is related to the variable  $x$  of the intrinsic charm quark in the proton, and according to the longitudinal momentum conservation law, the  $x_F \simeq x$  (and  $x_F < x$ ). Therefore, the visible excess of the inclusive spectrum, for example, of  $K$ -mesons can be due to the enhancement of the IS distribution (see Fig. 4) at  $x > 0.1$ .

The lower limits of the integration in (15) can be presented in the following form:

$$x_i^{\min} = \frac{x_R + x_F}{2 - (x_R - x_F)}, \quad x_j^{\min} = \frac{x_i(x_R - x_F)}{2x_i - (x_R + x_F)}, \quad (22)$$

where  $x_R = 2p/\sqrt{s}$ . One can see from (22) that, at least, one of the low limits  $x_i^{\min}$  of the integral (15) must be  $\geq x_F$ . Thus if  $x_F \geq 0.1$ , then  $x_i^{\min} > 0.1$ , where

the ordinary (extrinsic) charm distribution is completely negligible in comparison with the intrinsic charm distribution. Therefore, at  $x_F \geq 0.1$ , or equivalently at the charm momentum fraction  $x_c > 0.1$  the intrinsic charm distribution intensifies the charm PDF contribution into charm hadroproduction substantially (see Fig. 3). As a result, the spectrum of the open charm hadroproduction can be increased in a certain region of  $p_T$  and  $\eta$  (which corresponds to  $x_F \geq 0.1$  in accordance to 22). We stress that this excess (or even the very possibility to observe relevant events in this region) is due to the non-zero contribution of IC component at  $x_c > x_F > 0.1$  (where non-IC component completely vanishes).

This possibility was demonstrated for the  $D$ -meson production at the LHC in [66]. It was shown that the  $p_T$  spectrum of  $D$ -mesons is enhanced at pseudo-rapidities of  $3 < \eta < 5.5$  and  $10 \text{ GeV}/c < p_T < 25 \text{ GeV}/c$  due to the IC contribution, which was included using the CTEQ66c PDF [56]. For example, due to the IC PDF, with probability about 3.5 %, the  $p_T$ -spectrum increases by a factor of 2 at  $\eta = 4.5$ . A similar effect was predicted in [78].

One expects a similar enhancement in the experimental spectra of the open bottom production due to the (hidden) intrinsic bottom (IB) in the proton, which could have a distribution very similar to the one given in (12). However, the probability  $w_{\text{IB}}$  to find the Fock state with the IB contribution  $|uud\bar{b}\bar{b}\rangle$  in the proton is about 10 times smaller than the IC probability  $w_{\text{IC}}$  due to relation  $w_{\text{IB}}/w_{\text{IC}} \sim m_c^2/m_b^2$  [13, 36].

The IC “signal” can be studied not only in the inclusive open (forward) charm hadroproduction at the LHC, but also in some other processes, such as production of real prompt photons  $\gamma$  or virtual ones  $\gamma^*$ , or  $Z^0$ -bosons (decaying into dileptons) accompanied by  $c$ -jets in the kinematics available to the ATLAS and CMS experiments. The contributions of the heavy quark states in the proton could be investigated also in the  $c(b)$ -jet production accompanied by the vector bosons  $W^\pm$ ,  $Z^0$ . Similar kinematics given by (22) and (20) can also be applied to these hard processes.

In the next section we analyze in detail the hard process of the open strangeness production in  $pp$  collisions including the intrinsic strangeness (IS) contribution

in the proton.

#### 4. Intrinsic strangeness in proton

The BHPS model can be applied also for the search for the intrinsic strangeness (IS), see, for example, [68], where the early HERMES data [69] on the strange quark distribution  $xS(x, Q_0^2) = x[s(x, Q_0^2) + \bar{s}(x, Q_0^2)]$  at  $x > 0.1$  and  $Q_0^2 = 2.5$  (GeV/c)<sup>2</sup> has described rather satisfactorily using the IS contribution in a form about 2.5 %. Unfortunately later the new HERMES data appeared [79]. The HERMES information on  $xS(x, Q_0^2)$  were extracted from the data on the multiplicities of charged  $K$ -mesons produced in the deep inelastic  $ep$  scattering. The extraction of the polarization-averaged strange quark distribution from the HERMES data had an uncertainty related to the fragmentation functions (FFs). In Fig. 4 the old HERMES data [69] (circles) and the new ones (squares and triangles) are presented. The square points in Fig. 4 correspond to the FFs taken from [80] (DSS) and the triangles correspond to the following assumption:

$$\int D_S^K(z, Q_0^2) dz = 1.27, \quad (23)$$

where  $D_S^K(z, Q_0^2)$  is the FF of  $S$  to  $K \equiv K^+ + K^-$  (the sum of  $K^+$  and  $K^-$  mesons).

The dashed-dotted line in Fig. 4 corresponds to the PDF of type CTEQ6L [46], the dash curve is the IS contribution with its probability  $w_{IS} = 2.5$  % calculated within the BHPS model [6, 13]. One can see from Fig. 4 a large uncertainty of the HERMES data. Therefore, unfortunately the HERMES data do not allow to extract a reliable information on the IS contribution to the PDF of strange quarks.

Let us analyze now how the possible existence of the intrinsic strangeness in the proton can be visible in  $pp$  collisions. For example, consider the  $K^-$ -meson production in the process  $pp \rightarrow K^- + X$ . Considering the intrinsic strangeness in the proton [81] we calculated the inclusive spectrum  $d\sigma/d^3p$  of such mesons within the hard scattering model (Eq. (15)), which describes satisfactorily the

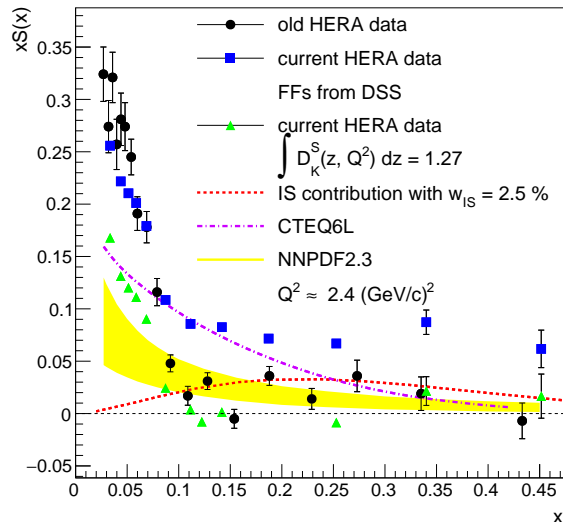


Figure 4: The distributions of strange quarks  $xS(x) = x(s(x) + \bar{s}(x))$  in the proton at  $Q^2 = 2.4 \text{ (GeV/c)}^2$ , the black points are the old HERMES data [69]; the blue squares are the new data [79], when the FFs are taken from [80] (DSS); the green triangles are the new data assuming the normalization given by Eq. (23); the dashed curve is the contribution of the intrinsic strangeness (IS) in the proton with the probability 2.5 %; the yellow band corresponds to NNPFD2.3 set [19].

HERA and HERMES data on the DIS. The FF and the parton cross-sections were taken from [82, 83], respectively, as mentioned above.

We also emphasize that the intrinsic  $s(x)$  and  $\bar{s}(x)$  are expected to be different in the proton since the comoving valence and strange quarks in the  $|uuds\bar{s}\rangle$  Fock state can repeatedly interact. This can also be understood by the duality of this Fock state with meson-nucleon fluctuations such as the  $K^+(\bar{s}u)\Lambda(uds)$  state. This duality [49] also predicts very different  $s(x)$  and  $\bar{s}(x)$  spin distributions in a polarized proton.

In Figs. 5, 6 the inclusive  $p_T$ -spectra of  $K^-$ -mesons produced in  $pp$  collision at the initial energy  $E_p = 158 \text{ GeV/c}$  are presented at the rapidity  $|y| = 1.3$  (Fig. 5) and  $|y| = 1.7$  (Fig. 6). The solid lines in Figs. 5, 6 correspond to our calculation ignoring the intrinsic strangeness (IS) in the proton and the dashed

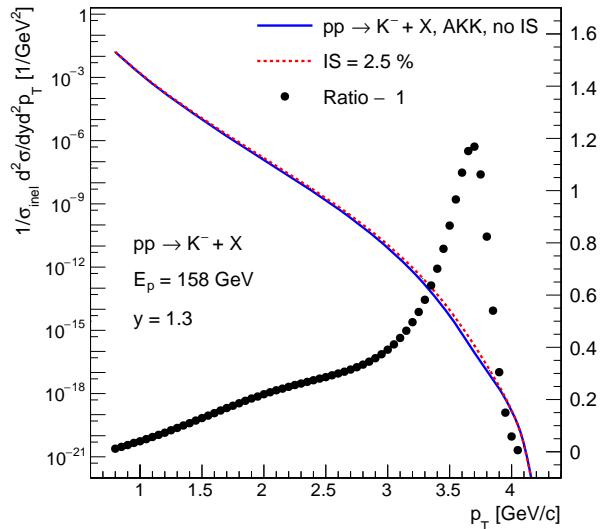


Figure 5: The  $K^-$ -meson distributions (with and without intrinsic strangeness contribution) over the transverse momentum  $p_T$  for  $pp \rightarrow K^- + X$  at the initial energy  $E = 158$  GeV/c, the rapidity  $y = 1.3$  and  $p_T \geq 0.8$  GeV/c.

curves correspond to the calculation including the IS with the probability about 2.5 %, according to [69]. The dots show the ratio of our calculation with the IS and without the IS minus 1. One can see from Figs. 5, 6 (right axis) that the IS signal can be above 200 % at  $|y| = 1.3$ ,  $p_T = 3.6 - 3.7$  GeV/c and slightly smaller, than 200 % at  $|y| = 1.7$ ,  $p_T \simeq 2.5$  GeV/c. Actually, this is our prediction for the NA61 experiment that is now under way at CERN.

## 5. Global analysis of PDFs with intrinsic charm

The charm content of the proton can be studied by the global analysis of PDFs, the charm quark distributions are generated perturbatively by pair radiation off gluons and light quarks, vanishing at a scale about the charm mass  $m_c$ , see details in [15, 18, 19, 84]. In contrast to this, it was found in [18] that the fitted charm PDF vanishes within uncertainties at a scale  $Q \sim 1.5$  GeV/c at  $x \leq 0.1$  independently of the  $m_c$  value. However, It was also shown [18] that,

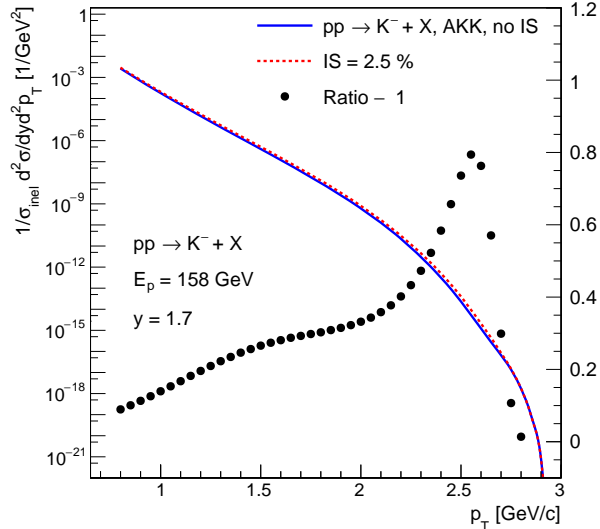


Figure 6: The  $K^-$ -meson distributions (with and without intrinsic strangeness contribution) over the transverse momentum  $p_T$  for  $pp \rightarrow K^- + X$  at the initial energy  $E = 158$  GeV/c, the rapidity  $|y| = 1.7$  and  $p_T \geq 0.8$  GeV/c.

at  $x \geq 0.1$  and low scales the charm PDF does not vanish and rather has an intrinsic component, very weakly scale dependent and almost independent of the  $m_c$  value, carrying about 1 % of the total proton momentum. The uncertainties in all other PDFs are slightly increased by including the IC charm, while the dependence of these PDFs on  $m_c$  is significantly reduced [18]. As was shown, the uncertainties in the fitted charm PDF are reduced if the EMC charm structure function data set is included. The main application of the results obtained in [18, 19, 84] for the LHC phenomenology is the increase stability respect to  $m_c$  persists at high scales.

The charm PDF can have a non-vanishing intrinsic component of the non-perturbative origin, see, for example, [15]. On the other hand, if one assumes that the charm PDF is purely perturbative in origin, it vanishes below its production threshold. The question arises as to the value of this threshold related to the charm pole mass, which is not known very precisely. Even if the charm is entirely perturbative and its production threshold is known, there is a prob-

lem of getting the accurate predictions because the cross-section of the massive charm is known within the low perturbative order. These difficulties are solved, for example, within the NNPDF3.0 set [19]. Within this set the charm PDF is parametrized on the basis of light quark and gluon PDFs, i.e., with an independent neural network with 37 free parameters.

## 6. Intrinsic heavy quark signal in processes at collider energies

### 6.1. Inclusive production of charmed meson

It was shown that the IC could result in a sizable contribution to the forward charmed meson production [67]. Furthermore the IC “signal” can constitute almost 100 % of the inclusive spectrum of  $D$ -mesons produced at high pseudo-rapidities  $\eta$  and large transverse momenta  $p_T$  in  $pp$  collisions at LHC energies [66].

If the distributions of the intrinsic charm or bottom in the proton are hard enough and are similar in the shape to the valence quark distributions (have the valence-like form), then the production of the charmed (bottom) mesons or charmed (bottom) baryons in the fragmentation region should be similar to the production of pions or nucleons. However, the yield of this production depends on the probability to find the intrinsic charm or bottom in the proton, but this yield appears to be rather small. The PDF which included the IC contribution in the proton have already been used in the perturbative QCD calculations in [16, 50, 56].

The possible existence of the intrinsic charm in the proton can lead to some enhancement in the inclusive spectra of the open charm hadrons, in particular  $D$ -mesons, produced at the LHC in  $pp$ -collisions at high pseudo-rapidities  $\eta$  and large transverse momenta  $p_T$  [66].

The inclusion of the intrinsic bottom or/and charm in the proton can increase the yield of the relevant heavy flavour baryons by a factor of 3 to 10. In particular, we considered a possibility of measuring the reaction  $pp \rightarrow \Lambda_c^+ X \rightarrow$

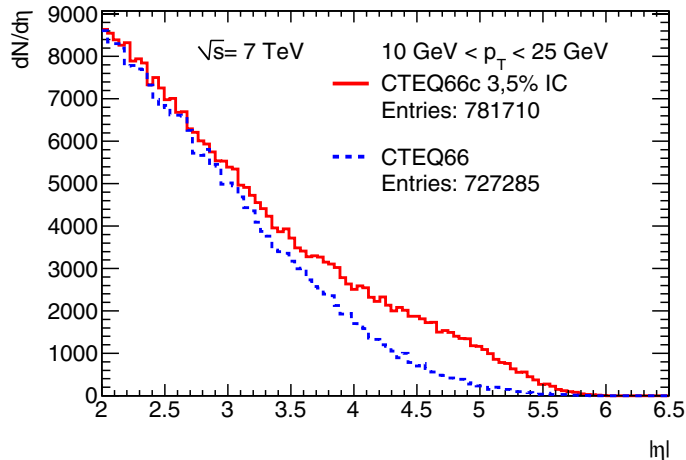


Figure 7: The  $D_0 + \bar{D}_0$  distributions over the pseudorapidity  $\eta$  in  $pp \rightarrow (D_0 + \bar{D}_0)X$  at  $\sqrt{s} = 7 \text{ TeV}/c$  and  $10 \leq p_T \leq 25 \text{ GeV}/c$  [66].

$\Lambda^0 \pi^+ X \rightarrow n \pi^0 \pi^+ X$  using the ATLAS, more specifically, one of its forward detectors the ZDC. This measurement can provide information on the intrinsic charm in the proton, the probability of which is estimated to be a factor of 10 higher than the one for the intrinsic bottom in the proton. Finally, it is worth noticing that any reliable non-observation of this enhancement in the experiments at the LHC can severely constrain the intrinsic heavy quark hypothesis.

Our calculations of the charmed meson production in  $pp$  collisions were done within the MC generator PYTHIA8 including the IC contribution with the probability about 3.5 % to the PDF are presented in Fig. 7 [66]. It is the distribution of the single  $D$ -mesons ( $D_0 + \bar{D}_0$ ) produced in the  $pp$  collision at  $\sqrt{s} = 7 \text{ TeV}/c$  as a function of their pseudo-rapidity  $\eta$ . We found that the contribution of the intrinsic charm in the proton could be studied in the production of  $D$ -mesons in  $pp$  collisions at the LHC. The IC contribution for the single  $D^0$ -meson production can be sizable, it is about 100 % at large rapidities  $3 \leq |y| \leq 4.5$  and large transverse momenta  $10 \leq p_T \leq 25 \text{ GeV}/c$ . As it is shown in [66], for the double  $D_0$  production this contribution is not larger than 30 % at  $p_T \geq 5 \text{ GeV}/c$  and  $3 \leq |y| \leq 4.5$ . These IC contributions for the single and double  $D$ -meson

production were obtained with the probability of the intrinsic charm taking to be  $w_{c\bar{c}} = 3.5\%$  [56], and they will decrease by a factor of 3 when  $w_{c\bar{c}} \simeq 1\%$ . Therefore, this value can be verified experimentally at LHCb.

The predictions presented in Fig. 7 [66] could be verified at the LHCb experiment in the kinematic region mentioned above to observe a possible signal for the intrinsic charm. The intrinsic bottom in the proton is suppressed by a factor of 10 [36], therefore its signal in the inclusive spectra of  $B$ -mesons will probably be very weak.

The IC contributions could be also observed at the SMOG experiment [85] of the LHCb in the production of the open charm, for example,  $D$ -mesons or charmed baryons  $\Lambda_c$ . One can use a gas jet target in a LHC detector — such as the SMOG target available at LHCb — to study novel intrinsic heavy quark physics phenomena in  $pA$  collisions. Remarkably, heavy-quark hadrons such as the  $\Lambda_b$ , double-charm baryons, and exotic hadrons such as tetraquarks and pentaquarks containing heavy quarks will be produced at small target rapidities — nearly at rest in the nuclear target rest frame — and thus can be easily observed. We note that the intrinsic heavy quark Fock states of a proton in the nuclear target, such as  $|uudQ\bar{Q}\rangle$ , have high light-front momentum fraction  $x_Q$ . The collision materializes the far off-shell light-front wave functions of Fock states, such as  $|uudb\bar{b}\rangle$ . The coalescence of the heavy quarks with the comoving light quarks corresponds to the production of a heavy hadron such as a  $\Lambda_b(udb)$  at *small rapidity*  $|y_{\Lambda_b}| \simeq \ln x_b$ , relative to the rapidity of the nucleon in the target.

### 6.2. Inclusive production of Higgs boson and intrinsic charm and bottom in proton

The interesting predictions on the possible signal of the intrinsic heavy quark (IQ) contributions to the inclusive  $x_F$ -spectrum of the Higgs bosons produced at the TEVATRON and LHC energies are presented in [42]. In Fig. 8 the contributions of the IC and IB to the  $x_F$ -distribution of the Higgs boson produced in  $pp$  collisions at the collider energies LHC and TEVATRON are presented.

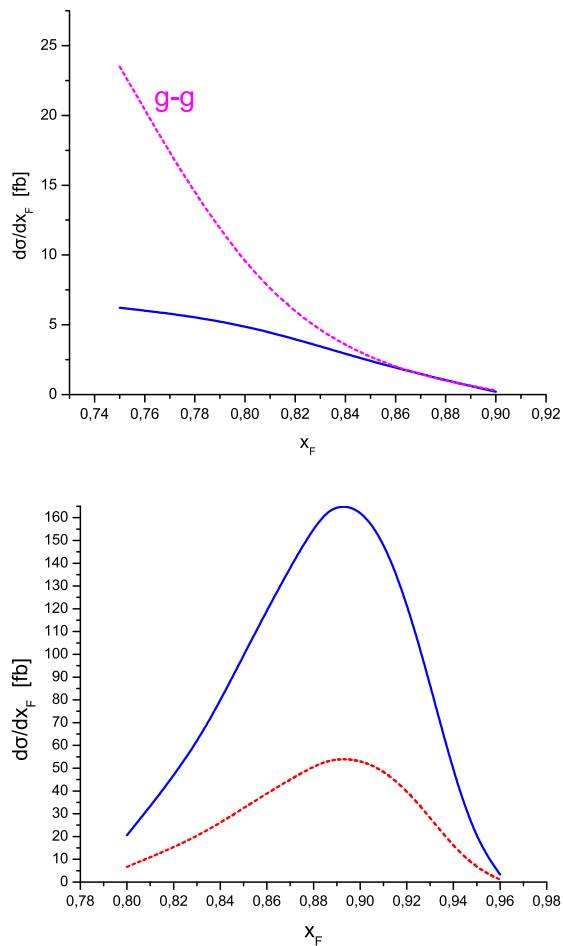


Figure 8: The  $x_F$ -distribution of the Higgs boson produced in  $pp$  collision at the LHC energy  $\sqrt{s} = 14$  TeV/c due to the non-perturbative intrinsic charm with the probability about 1 % (solid line). The dashed line corresponds to the Higgs boson production from the gluon-gluon fusion (top). The same distribution due to the non-perturbative intrinsic bottom (IB) at the LHC energy  $\sqrt{s} = 14$  TeV/c (solid line) and the TEVATRON energy  $\sqrt{s} = 2$  TeV (dashed line, bottom) [42].

One can see from Fig. 8 that the  $x_F$ -distribution for the inclusive Higgs boson production coming from the IB contribution is much larger than the one coming from the IC. It is due to the fact that the Higgs- $Q$  coupling is proportional to

the quark mass  $m_Q$ , therefore the Higgs- $b$  coupling constant is much larger than the coupling constant Higgs- $c$ . Fig. 8 also shows that the cross section  $d\sigma/dx_F$  for the inclusive production of the Standard Model Higgs boson coming from the IB is of order 150 fb at the LHC energy  $\sqrt{s} = 14$  TeV/c, peaking in the region of  $x_F \simeq 0.9$ . Therefore, the signal of the IB in the differential cross section of the Higgs boson produced in  $pp$  collision at high  $x_F$  can be tested at the LHC. As is shown in [42], it is much larger than the IC signal.

### 6.3. Production of prompt photon and $c$ or $b$ -jet in hard $pp$ collisions

The investigation of prompt photon and  $c(b)$ -jet production in  $p\bar{p}$  collisions at  $\sqrt{s} = 1.96$  TeV/c was carried out at the TEVATRON [31–34]. In particular, it was observed that the ratio of the experimental spectrum of the prompt photons accompanied by the  $c$ -jets to the relevant theoretical expectation (based on the conventional PDF, which ignored the IC contribution) increases up to factor of about 3, when  $p_T^\gamma$  becomes above 110 GeV/c. Furthermore, taking into account the CTEQ66c PDF, which includes the IC contribution obtained within the BHPS model [6, 13] one can reduce this ratio up to 1.5 [37]. For the  $\gamma + b$ -jets  $p\bar{p}$ -production no enhancement in the  $p_T^\gamma$ -spectrum was observed at the beginning of the experiment [31, 34]. However, in 2012 the DØ collaboration has confirmed observation of such an enhancement [32]. It is illustrated in Fig. 9.

The dash-dotted lines in Fig. 9 (bottom) show the ratio between the NLO calculations of  $p_T^\gamma$ -spectrum obtained within the BHPS model (using the CTEQ66c with the IC probability about 3.5 %) and the spectrum using the CTEQ6M without the IC contribution. In addition to that the IC signal was visible in the ratio between the differential cross-sections of the photon and  $c$ -jet production in  $p\bar{p}$  collision,  $\gamma + c$ , and  $\gamma + b$  production, see Fig. 10. This figure shows that, according to the pQCD calculations [37], in the absence of the IC contribution this ratio decreases (solid line), as  $p_T^\gamma$  grows, while the TEVATRON data show its flat behavior at large  $p_T \geq 100$  GeV/c. As for the prompt photon production accompanied by the  $b$ -jet in  $p\bar{p}$  annihilation, the TEVATRON data do not show any signal of the intrinsic  $b$  contribution, see Fig. 9 (top) [31]. It can be due to

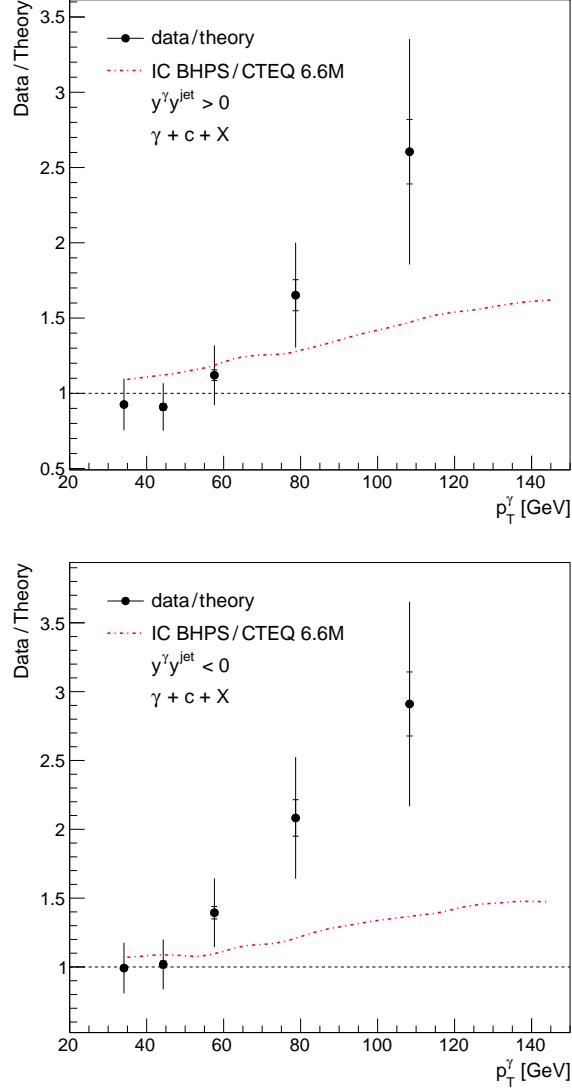


Figure 9: The data-to-theory ratio [31] for the processes  $p\bar{p} \rightarrow \gamma + c + X$ , when  $y^\gamma y^{\text{jet}} > 0$  (top) and the same ratio, when  $y^\gamma y^{\text{jet}} < 0$  (bottom) at  $\sqrt{s} = 1.96$  TeV/c. The dash-dotted line is the calculation of this ratio using the BHPs IC model with the IC probability about 3.5 %.

very small intrinsic bottom probability in a proton, as mentioned above.

This intriguing observation stimulates our interest to look for a similar IC

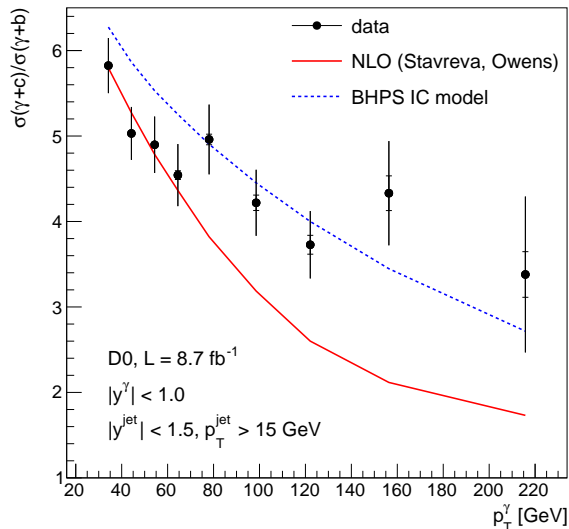


Figure 10: The ratio  $\sigma(\gamma + c)/\sigma(\gamma + b)$  as a function of the photon transverse momentum  $p_T^\gamma$  in  $p\bar{p} \rightarrow \gamma + c(b) + X$  process at  $\sqrt{s} = 1.96$  TeV/c, see [33].

signal in  $pp \rightarrow \gamma + c(b) + X$  processes at LHC energies, see [38, 40].

The Examples of Feynman diagrams corresponding to  $gg \rightarrow \gamma(Z)Q\bar{Q}$  (a),  $q\bar{q} \rightarrow \gamma(Z)Q\bar{Q}$  (b,c) and  $qQ \rightarrow \gamma(Z)qQ$  (d,e) subprocesses are presented in Fig. 11.

The diagrams within the NLO QCD are more complicated than Fig. 11.

Let us illustrate qualitatively the kinematical regions where the IC component can contribute significantly to the spectrum of prompt photons produced together with a  $c$ -jet in  $pp$  collisions at the LHC. For simplicity we consider only the contribution to the reaction  $pp \rightarrow \gamma(Z) + Q + X$  of the diagrams given in Fig. 11 (a). According to (20) at certain values of the transverse momentum of the photon,  $p_T^\gamma$ , and its pseudo-rapidity,  $\eta^\gamma$ , (or rapidity  $y^\gamma$ ) the momentum fraction of  $\gamma$  can be  $x_F^\gamma > 0.1$ , therefore the fraction of the initial  $c$ -quark must also be above 0.1, where the IC contribution in the proton is enhanced (see Fig. 3). Therefore, one can expect some non-zero IC signal in the  $p_T^\gamma$  spectrum of the reaction  $pp \rightarrow \gamma + c + X$  in this certain region of  $p_T^\gamma$  and  $y^\gamma$  [38]. A similar

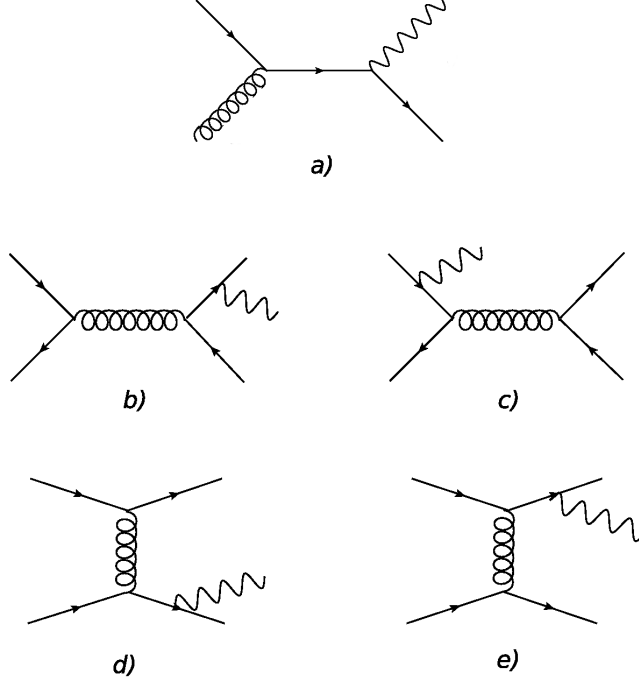


Figure 11: The  $\mathcal{O}(\alpha\alpha_s)$  (a) and  $\mathcal{O}(\alpha\alpha_s^2)$  (b) – (e) contributions to the  $\gamma(Z) + Q$  production.

IC effect can be visible in the production of the  $Z$  or  $W$ -boson accompanied by  $c$  or  $b$ -jets in  $pp$  collisions. In [39, 40] the theoretical predictions about the possible observation of the IC signal in the  $p_T$ -spectra of  $Z$  or  $W$ -bosons accompanied by the  $c$  or  $b$ -jets respectively are presented. These processes will be considered later. First, let us discuss a possible search for the IC signal in the production of prompt photons accompanied by  $c$ -jet in  $pp$  collision at LHC energies.

In Fig. 12 the differential cross-section  $d\sigma/dp_T^\gamma$  calculated at NLO within the collinear QCD massless quark approximation as described in [37] is presented as a function of the transverse momentum of the prompt photon [38]. The following requirements are applied:  $p_T^\gamma > 45$  GeV/c,  $p_T^c > 20$  GeV/c with the  $c$ -jet pseudorapidity in the interval  $|y_c| \leq 2.4$  and the photon pseudorapidity in the interval  $1.52 < |y_\gamma| < 2.37$  (forward region). The solid line represents the differential cross-section calculated with the radiatively generated charm PDF

(CTEQ66), the dash-dotted line uses as input the sea-like PDF (CTEQ66c4) and the dashed line the BHPS PDF (CTEQ66c2). In the lower half of Fig. 12 the above distributions normalized to the distribution acquired using the CTEQ66 PDF and  $\mu_r = \mu_f = \mu_F = p_T^\gamma$ , are presented. The shaded yellow region, represents the scale dependence. Clearly the difference between the spectrum using the BHPS IC PDF and the one using the radiatively generated PDF increases as  $p_T^\gamma$  grows.

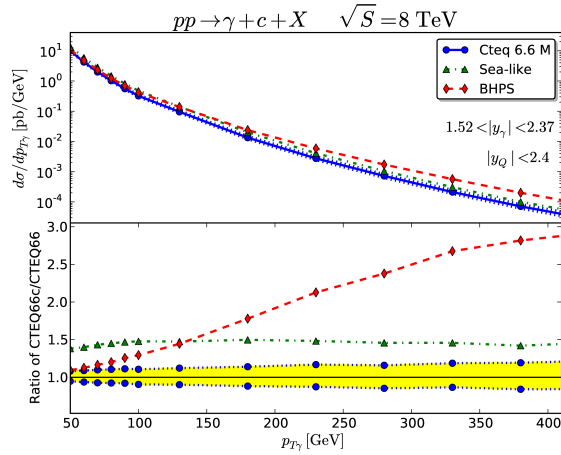


Figure 12: The  $d\sigma/dp_T^\gamma$  distribution versus the transverse momentum of the photon for the process  $pp \rightarrow \gamma + c + X$  at  $\sqrt{s} = 8\text{TeV}/c$  using CTEQ6.6M (solid blue line), BHPS CTEQ6c2 (dashed red line) and sea-like CTEQ6c4 (dash-dotted green line), for forward photon rapidity  $1.52 < |y_\gamma| < 2.37$ . The ratio of these spectra with respect to the CTEQ6.6M (solid blue line) distributions (bottom). The calculation was done within the NLO QCD approximation.

Therefore, Fig. 12 shows that the IC signal could be visible at the LHC energies with both the ATLAS and CMS detector in the process  $pp \rightarrow \gamma + c + X$  when  $p_T^\gamma \simeq 150 \text{ GeV}/c$ . In the region described above the IC signal dominates over the all non-intrinsic charm background with significance at a level of a factor of 2 (in fact 170 %).

#### 6.4. Production of $\gamma(Z) + c(b)$ -jet within the $k_T$ -factorization and the MCFM

The  $k_T$ -factorization approach [86–88] is based on the small- $x$  Balitsky-Fadin-Kuraev-Lipatov (BFKL) [89–91] gluon dynamics and provides solid theo-

retical ground for the effects of the initial gluon radiation and the intrinsic parton transverse momentum.<sup>1</sup> Our main motivation to use the  $k_T$ -factorization formalism here is that its predictions for the associated  $\gamma + Q$  production better agree with the TEVATRON data compared to the NLO pQCD (see [32, 35]). The consideration is mainly based on the  $\mathcal{O}(\alpha\alpha_s)$  off-shell (depending on the transverse momenta of initial quarks and gluons) quark-gluon Compton-like scattering subprocess, see Fig. 11 (a). Within this approach the transverse momentum dependent (TMD) parton densities include many high order corrections, while the partonic amplitudes are calculated within the leading order (LO) of QCD. The off-shell quark-gluon Compton scattering amplitude is calculated within the reggeized parton approach [95–99] based on the effective action formalism [100, 101], which ensures the gauge invariance of the obtained amplitudes despite the off-shell initial quarks and gluons.<sup>2</sup> The TMD parton densities are calculated using the Kimber-Martin-Ryskin (KMR) approach, currently developed within the NLO [103]. This approach is the formalism to construct the TMD quark and gluon densities from the known conventional parton distributions. The key assumption is that the  $k_T$  dependence appears at the last evolution step, so that the DGLAP evolution can be used up to this step. Numerically, for the input we used parton densities derived in Section 2. Other details of these calculations are explained in [102].

To improve the  $k_T$ -factorization predictions at high transverse momenta, we take into account some  $\mathcal{O}(\alpha\alpha_s^2)$  contributions, namely  $q\bar{q} \rightarrow VQ\bar{Q}$  and  $qQ \rightarrow VqQ$  ones, where  $V$  denotes the photon or the  $Z$  boson, see Fig. 11 ((b) – (e)). These contributions are significant at large  $x$  and therefore can be calculated in the usual collinear QCD factorization scheme. Thus, we rely on the combination of two techniques that are most suitable.

Let us present the results of our calculations. First of all we describe our nu-

---

<sup>1</sup>A detailed description of the  $k_T$ -factorization approach can be found, for example, in reviews [92–94]

<sup>2</sup>Here we use the expressions derived earlier [102].

merical input. Following to [103], we set the charmed and bottom quark masses  $m_c = 1.4 \text{ GeV}/c$ ,  $m_b = 4.75 \text{ GeV}/c$ , the  $Z$ -boson mass  $m_Z = 91.1876 \text{ GeV}/c$ , and  $\sin^2 \theta_W = 0.23122$ . The chosen factorization and renormalization scales are  $\mu_R = \mu_F = \xi p_T$  or  $\mu_R = \mu_F = \xi m_T$ , where  $p_T$  is the produced photon transverse momentum and  $m_T$  is the  $Z$  boson transverse mass. As usual, we vary the non-physical parameter  $\xi$  between  $1/2$  and  $2$  about the default value  $\xi = 1$  in order to estimate the scale uncertainties of our calculations. We employ the two-loop formula for the strong coupling constant with active quark flavors  $n_f = 5$  at  $\Lambda_{\text{QCD}} = 226.2 \text{ MeV}/c$  and use the running QED coupling constant over a wide region of transverse momenta. The multidimensional integration in the  $k_T$ -factorization calculations was performed by means of the Monte Carlo technique, using the VEGAS routine [104].

In our calculations we also follow the conclusion obtained in our papers [38, 39] that the IC signal in the hard processes discussed here can be detected at ATLAS or CMS of the LHC in the forward rapidity region  $1.5 < |\eta| < 2.4$  and  $p_T > 50 \text{ GeV}/c$ . Additionally, we require  $|\eta(Q)| < 2.4$  and  $p_T(Q) > 25 \text{ GeV}/c$ , where  $\eta(Q)$  and  $p_T(Q)$  are the pseudo-rapidity and transverse momentum of the heavy quark jet in a final state, as was done in [38, 39].

The results of our calculations are shown in Figs. 13 – 21. The transverse momentum distributions of photons and  $Z$  bosons accompanied by the  $c$  and  $b$  quarks are presented in Figs. 13, 14 and 15 at the different IC probability  $w$  (namely,  $w = 0 \%$ ,  $w = 2 \%$  and  $w = 3.5 \%$ ) at  $\sqrt{s} = 8$  and  $13 \text{ TeV}/c$ .

One can see in Figs. 14 and 15 that the MCFM and  $k_T$ -factorization predictions for  $Z + Q$  production are very similar in the whole  $p_T$  region, therefore below we will present the observables calculated within the  $k_T$ -factorization approach only. The coincidence of these two calculations is due to effective allowance for the high-order corrections within the  $k_T$ -factorization formalism (see, for example, [92–94] for more information). Both types of calculations predict a significant enhancement of  $p_T$  distributions due to the IC terms at  $p_T \geq 100 \text{ GeV}/c$ , which is in agreement with the previous studies [38, 39, 64].

The  $p_T$  spectrum ratios  $\sigma(\gamma + c)/\sigma(\gamma + b)$  and  $\sigma(Z + c)/\sigma(Z + b)$  versus  $p_T$

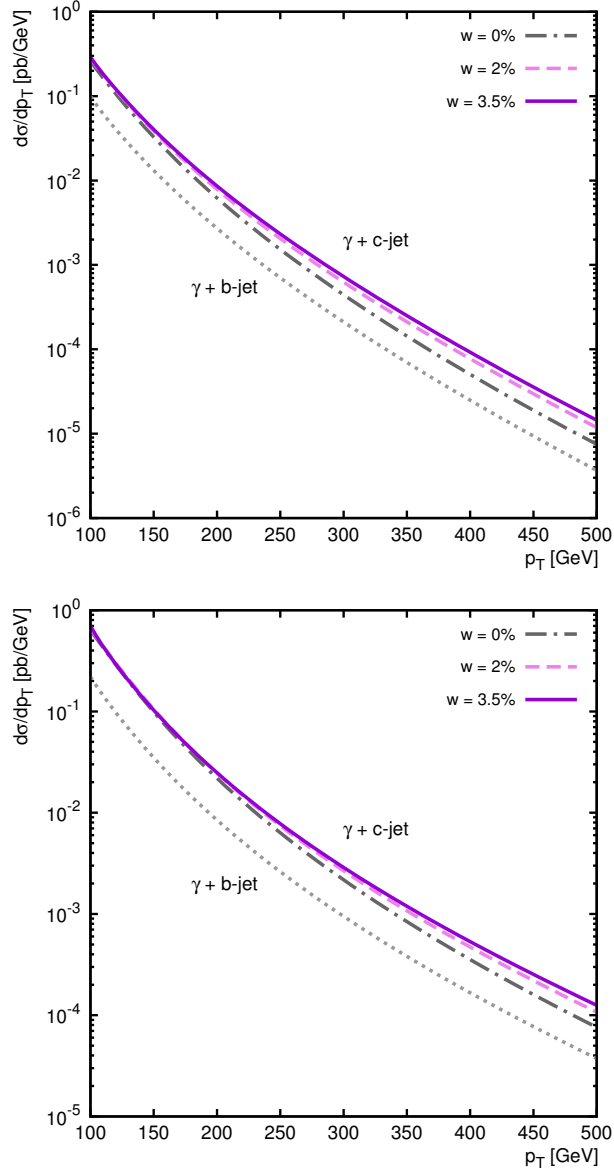


Figure 13: The cross-sections of the associated  $\gamma + c$  and  $\gamma + b$  production in the  $pp$  collision calculated as a function of the photon transverse momentum  $p_T$  at  $\sqrt{s} = 8$  TeV/c (top) and  $\sqrt{s} = 13$  TeV/c (bottom) within the  $k_T$ -factorization approach. The kinematical conditions are described in the text.

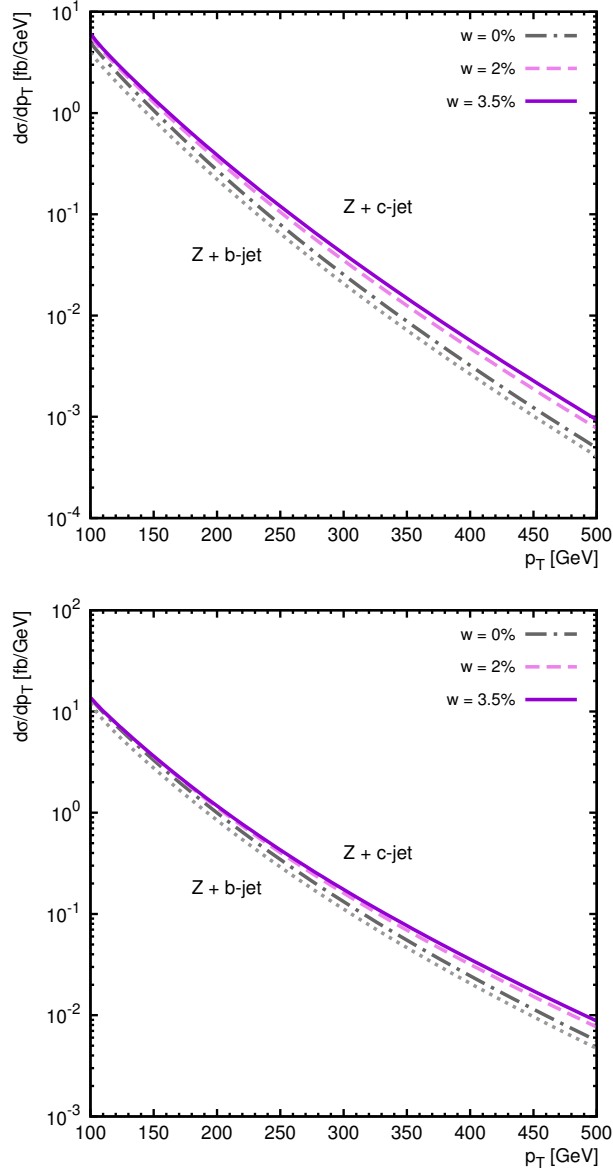


Figure 14: The cross-sections of the associated  $Z + c$  and  $Z + b$  production in the  $pp$  collision calculated as a function of the  $Z$  boson transverse momentum  $p_T$  at  $\sqrt{s} = 8$  TeV/c (top) and  $\sqrt{s} = 13$  TeV/c (bottom) within the  $k_T$ -factorization approach. The kinematical conditions are described in the text.

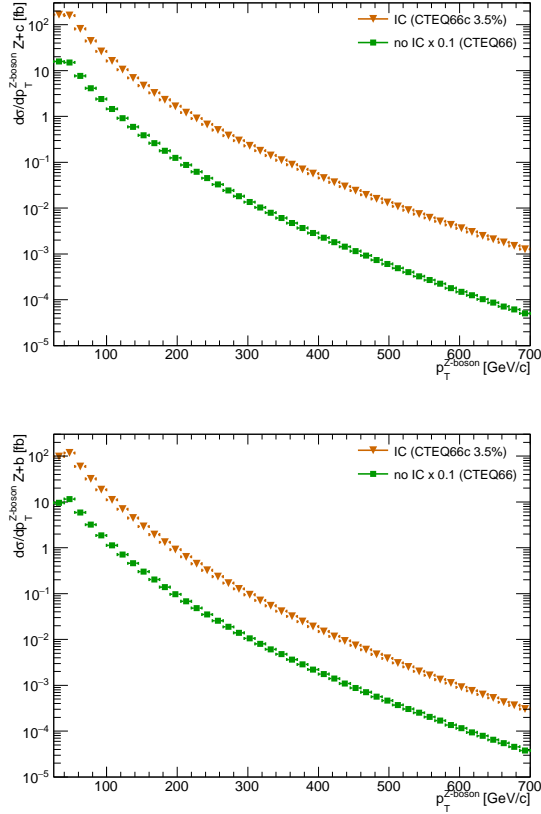


Figure 15: The cross-sections of the associated  $Z+c$  (top) and  $Z+b$  (bottom) production in  $pp$  collision calculated as a function of the  $Z$  boson transverse momentum  $p_T$  at  $\sqrt{s} = 13$  TeV/ $c$  within the MCFM routine.

at different  $w$  are presented in Figs. 16 and 17. One can see that in the absence of the IC contribution the ratio  $\sigma(\gamma+c)/\sigma(\gamma+b)$  is about 3 at  $p_T \sim 100$  GeV/ $c$  and decreases down to 2 at  $p_T \sim 500$  GeV/ $c$ . This behavior is the same for both energies  $\sqrt{s} = 8$  TeV/ $c$  and  $\sqrt{s} = 13$  TeV/ $c$ .

If one takes into account the IC contributions, this ratio becomes approximately flat at  $w = 2$  % or even increasing up to about 4 at  $w = 3.5$  %. It is very close to the TEVATRON data [33]: the constant ratio  $\sigma(\gamma+c)/\sigma(\gamma+b) \sim 3.5 - 4.5$  measured in the  $p\bar{p}$  collisions at  $110 < p_T < 300$  GeV/ $c$  and

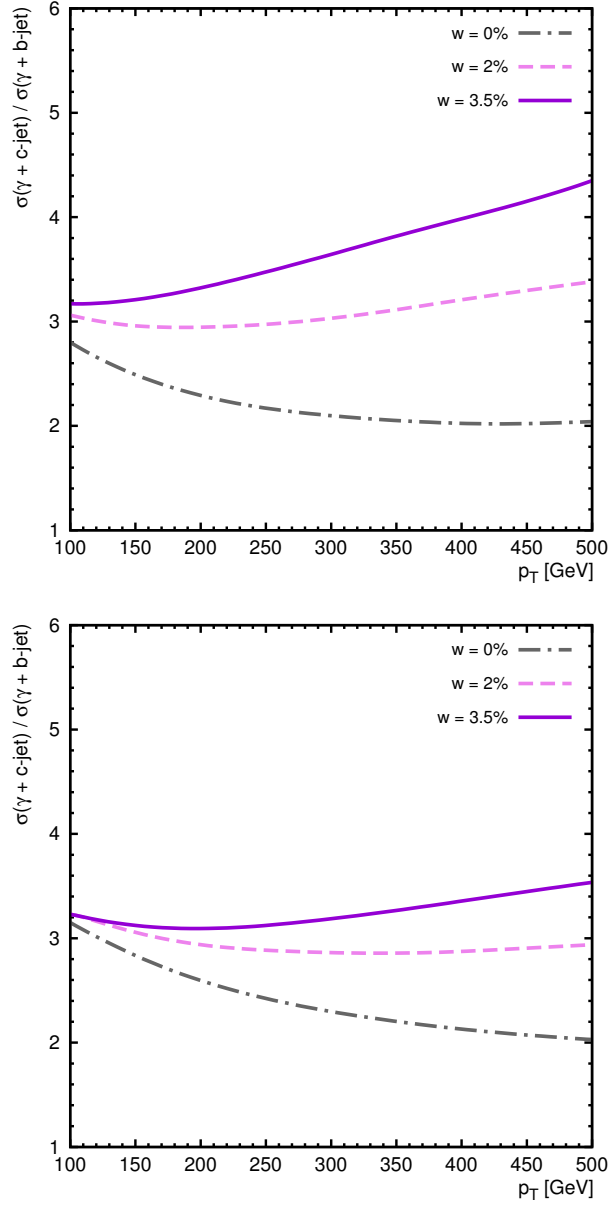


Figure 16: The cross-section ratio of the  $\gamma + c$  production to the  $\gamma + b$  one in the  $pp$  collision calculated as a function of the photon transverse momentum  $p_T$  at  $\sqrt{s} = 8$  TeV/c (top) and  $\sqrt{s} = 13$  TeV/c (bottom) within the  $k_T$ -factorization approach.

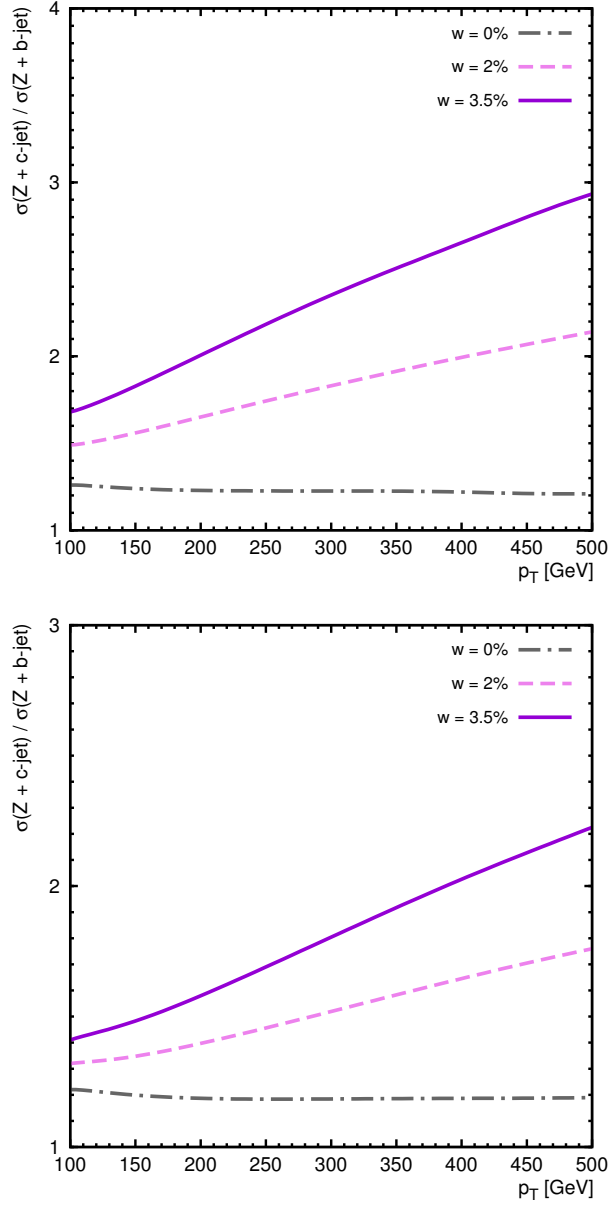


Figure 17: The cross-section ratio of the  $Z + c$  production to the  $Z + b$  one in the  $pp$  collision calculated as a function of the  $Z$  boson transverse momentum  $p_T$  at  $\sqrt{s} = 8$  TeV/c (top) and  $\sqrt{s} = 13$  TeV/c (bottom) within the  $k_T$ -factorization approach.

$\sqrt{s} = 1.96$  TeV/c. However, this agreement cannot be treated as the IC indication due to huge experimental uncertainties (about 50 %) and rather different kinematical conditions. If the IC contribution is included, the ratio  $\sigma(Z + c)/\sigma(Z + b)$  also increases by a factor about 2 at  $w = 3.5$  %, when the  $Z$  boson transverse momentum grows from 100 GeV/c to 500 GeV/c (see Fig. 17). In the absence of the IC terms this ratio slowly decreases.

One can consider other observables which could be useful to detect the IC signal, the cross-sections discussed above but integrated over  $p_T > p_T^{\text{min}}$ , where  $p_T^{\text{min}} \geq 100$  GeV/c, and their ratios. Our predictions for such integrated cross-sections versus the IC probability  $w$  at  $p_T^{\text{min}} = 100, 200$  and  $300$  GeV/c for  $\sqrt{s} = 8$  TeV/c and  $p_T^{\text{min}} = 200, 300$  and  $400$  GeV/c for  $\sqrt{s} = 13$  TeV/c are shown in Figs. 18, 19 and Figs. 20, 21.

All the  $p_T$ -spectra have a significant scale uncertainty as is shown in [39]. According to [39], the ratio between the cross-sections for the  $Z+Q$  and  $W+Q$  production in the  $pp$  collision is less sensitive to the scale variation calculated within the MCFM. Nevertheless, the uncertainty in this ratio at large  $p_T > 250$  GeV/c is about 40 – 50 %. In the present paper we check these results for the ratios  $\sigma(\gamma+c)/\sigma(\gamma+b)$  and  $\sigma(Z+c)/\sigma(Z+b)$ . In Figs. 18, 19 and Figs. 20, 21 we present these ratios versus the IC probability  $w$  calculated at different scales, when the cross-sections of  $\gamma(Z) + Q$  production are integrated within the different intervals of transverse momentum. One can see a very small QCD scale uncertainty, especially at  $\sqrt{s} = 13$  TeV/c (bottom right), which is less than 1 %. In contrast, the scale uncertainty for the integrated  $\gamma(Z) + Q$  cross-sections (see Figs. 18, 19 and Figs. 20, 21) is significant and amounts to about 30 – 40 %. The sizable difference between the scale uncertainties for the ratios  $\sigma(Z+Q)/\sigma(W+Q)$  and  $\sigma(Z+c)/\sigma(Z+b)$  is due to the different matrix elements for the  $Z+Q$  and  $W+Q$  production in  $pp$  collisions, while the matrix elements for the  $Z+c$  and  $Z+b$  production are the same.

It is important that the calculated ratios  $\sigma(\gamma+c)/\sigma(\gamma+b)$  and  $\sigma(Z+c)/\sigma(Z+b)$  can be used to determine the IC probability  $w$  from the future LHC data. Moreover, these ratios are practically independent of the uncertainties of our

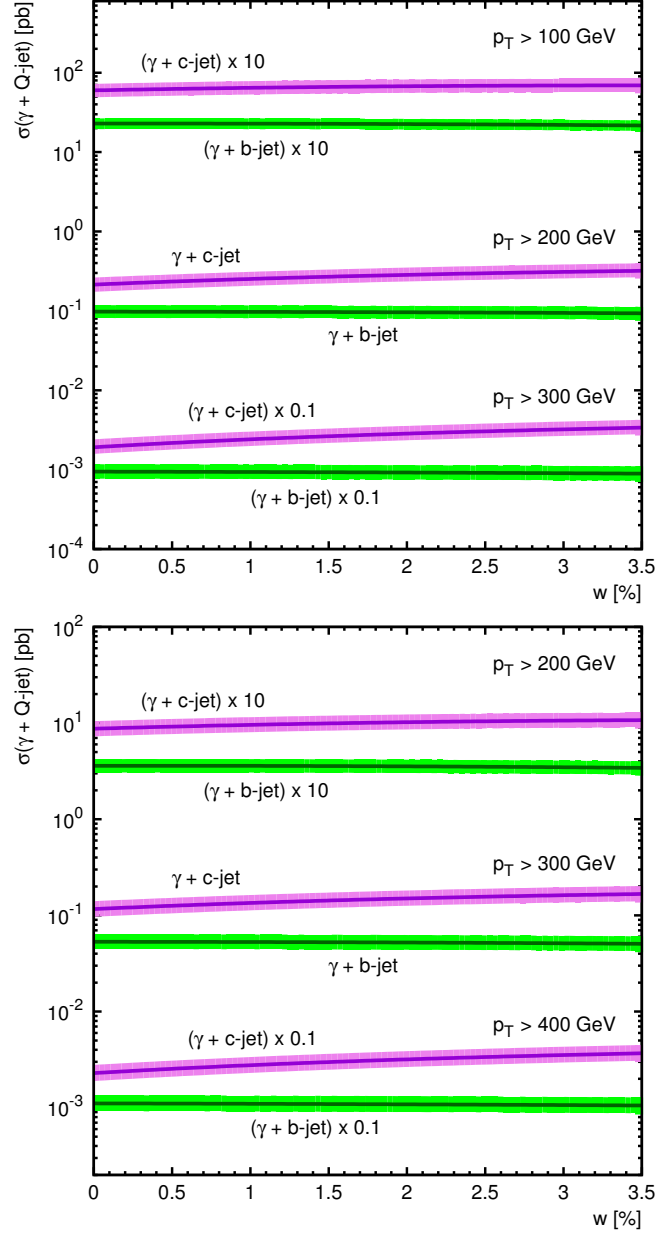


Figure 18: The cross-sections of the associated  $\gamma + c$  and  $\gamma + b$  production in the  $pp$  collision as a function of  $w$  integrated over the photon transverse momenta  $p_T > p_T^{\min}$  for different  $p_T^{\min}$  at  $\sqrt{s} = 8$  TeV/c (top) and  $\sqrt{s} = 13$  TeV/c (bottom).

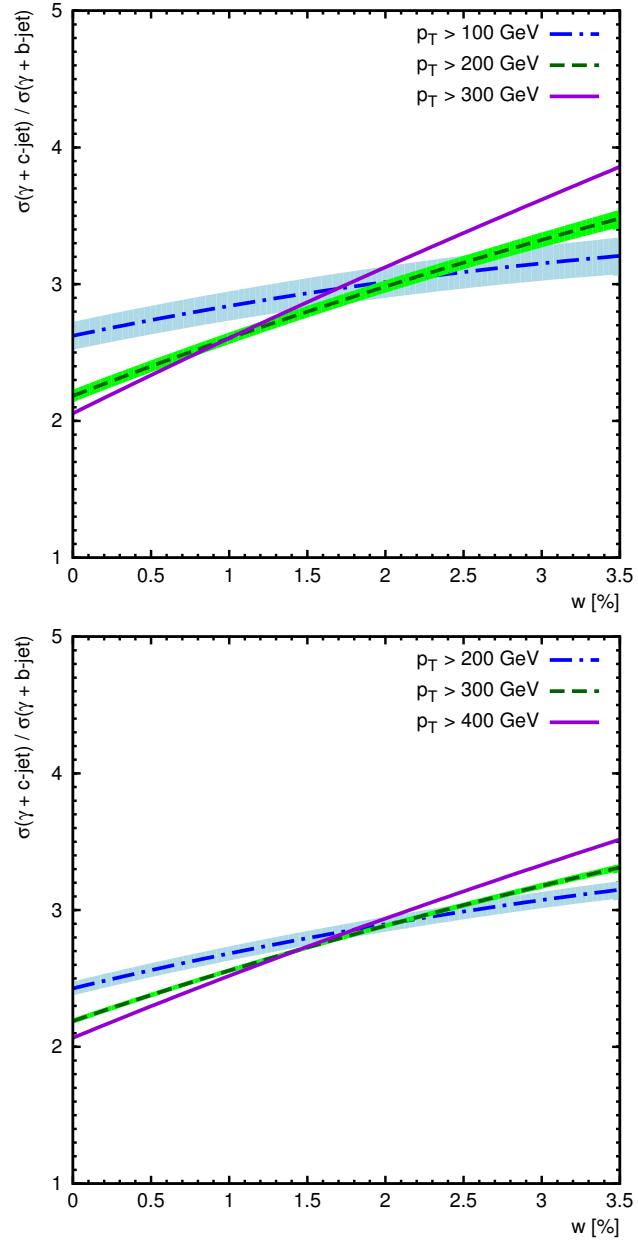


Figure 19: The corresponding ratios of these cross-sections. The calculations were done using the  $k_T$ -factorization approach. The bands correspond to the usual scale variation as it is described in the text.

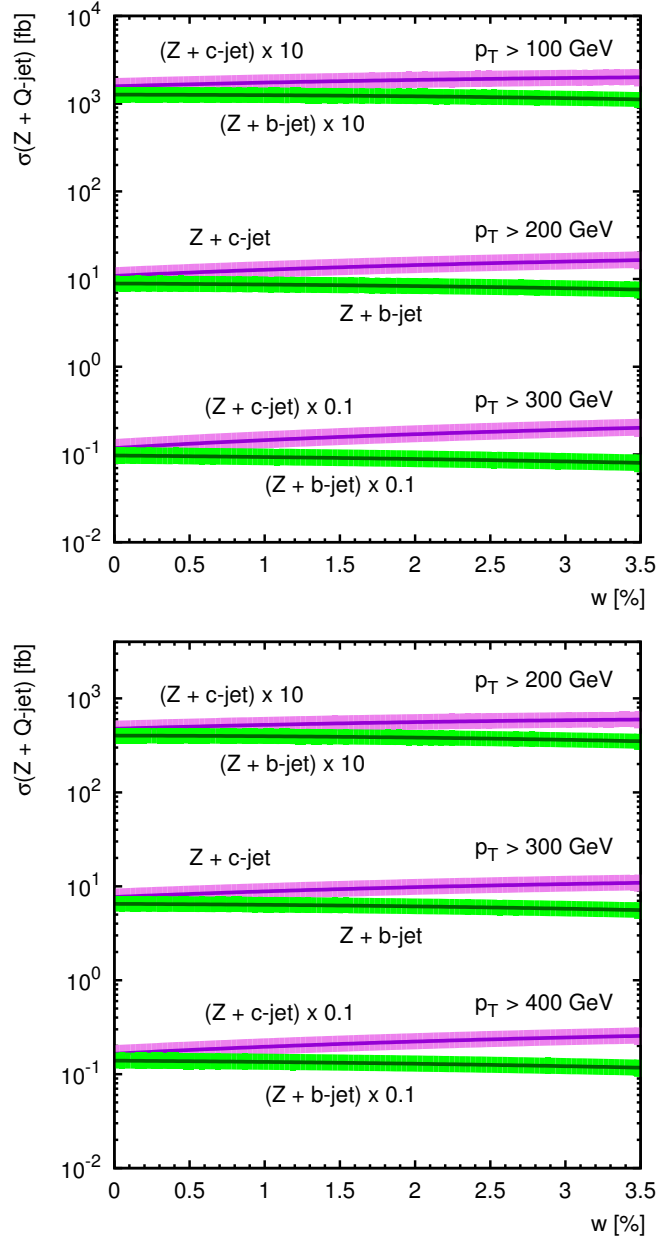


Figure 20: The cross-sections of the associated  $Z + c$  and  $Z + b$  production in the  $pp$  collision as a function of  $w$  integrated over the  $Z$  boson transverse momenta  $p_T > p_T^{\min}$  for different  $p_T^{\min}$  at  $\sqrt{s} = 8$  TeV/c (top) and  $\sqrt{s} = 13$  TeV/c (bottom). The kinematical conditions are described in the text.

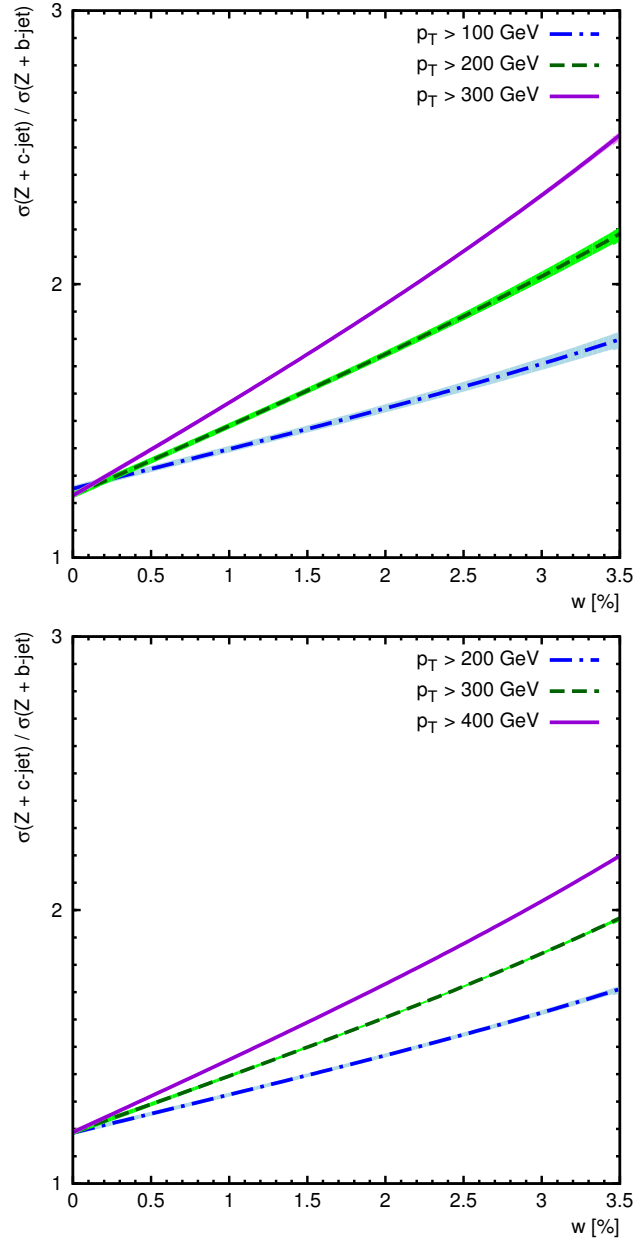


Figure 21: The corresponding ratios of these cross-sections. The calculations were done using the  $k_T$ -factorization approach. The bands correspond to the usual scale variation as it is described in the text.

calculations: actually, the curves corresponding to the usual scale variations as described above coincide with each other (see Figs. 19 and 21, bottom). Therefore, we can recommend these observables as a test for the hypothesis of the IC component inside the proton.

### 6.5. Prompt photon and open charm production

In Fig. 22 the differential cross-sections of prompt photons accompanied by the  $D^*$ -mesons calculated as a function of produced photon transverse momenta at  $\sqrt{s} = 8$  TeV/c (top) and 13 TeV/c (bottom) are presented with and without the IC contribution, and the ratios of these spectra are shown in Fig. 23. The calculations were performed using the  $k_T$ -factorization approach and the kinematical requirements applied are the same as above. We produce  $D^*$  mesons from charmed quarks using the Peterson fragmentation function with a shape parameter  $\epsilon_c = 0.06$ , and the branching fraction  $f(c \rightarrow D^*)$  is equal to 0.255. In Fig. 23 the ratio of the  $p_T$ -spectra of the photons accompanied by the  $D^*$  mesons in  $pp$  collisions with the intrinsic 3.5 % charm contribution and without it at  $\sqrt{s} = 8$  TeV/c (top) and  $\sqrt{s} = 13$  TeV/c (bottom). One can see that the IC signal in the  $\gamma + D^*$  cross-section is practically the same as in the case of  $\gamma + c$ -jet production.

### 6.6. $W(Z)$ -boson and $b(c)$ -jet production

Let us analyze another hard processes of the production of vector boson accompanied by the  $b$  and  $c$  jets in  $pp$  collision, which can give us also information on the intrinsic charm in proton [39]. The LO QCD diagram for the process  $Q_f(\bar{Q}_f) + g \rightarrow Z^0 + Q_f(\bar{Q}_f)$  is presented in Fig. 24. These hard subprocesses can give the main contribution to the reaction  $pp \rightarrow Z^0(\rightarrow l^+ + l^-) + Q_f(\bar{Q}_f) - jet + X$ , which could also give us information on the IC contribution in the proton.

The LO QCD diagram for the process  $Q_f(\bar{Q}_f) + g \rightarrow W^\pm + Q'_f(\bar{Q}'_f)$  is presented in Fig. 25, where  $Q_f = c, b$  and  $Q'_f = b, c$ . These hard subprocesses can give the main contribution to the reaction  $pp \rightarrow W^\pm(\rightarrow l^+ + \nu) + Q'_f(\bar{Q}'_f) - jet + X$ ,

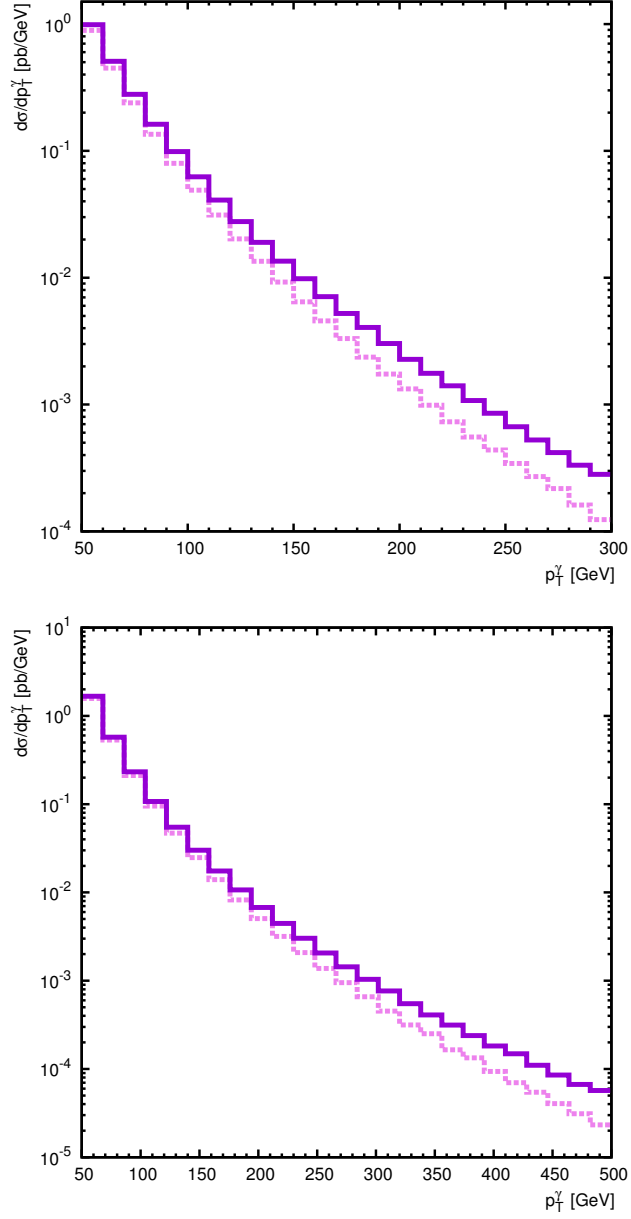


Figure 22: The  $p_T$ -spectra of the photons accompanied by the  $D^*$ -mesons in  $pp$  collisions with the intrinsic 3.5 % charm contribution and without it at  $\sqrt{s} = 8$  TeV/c (top) and  $\sqrt{s} = 13$  TeV/c (bottom). Both plots correspond to  $1.5 < |y^\gamma| < 2.4$ ,  $|y^{\text{jet}}| < 2.4$ .

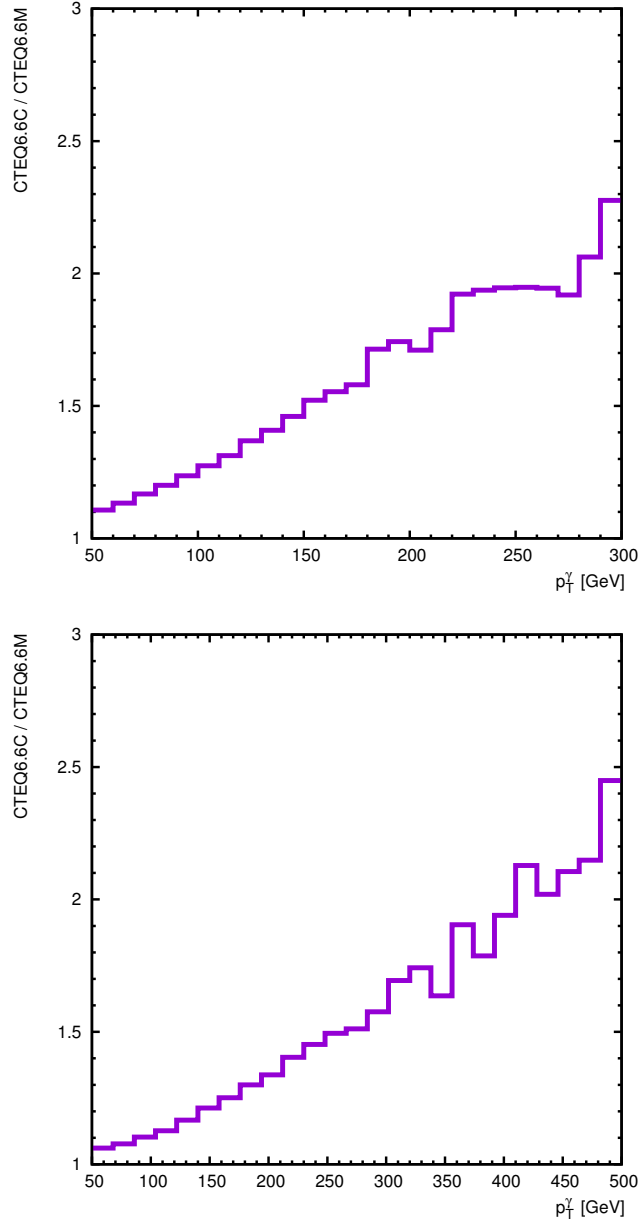


Figure 23: The ratios of the  $p_T$ -spectra of the photons accompanied by the  $D^*$ -mesons in  $pp$  collisions with the intrinsic 3.5 % charm contribution and without it at  $\sqrt{s} = 8$  TeV/c (top) and  $\sqrt{s} = 13$  TeV/c (bottom). Both plots correspond to  $1.5 < |y^\gamma| < 2.4$ ,  $|y^{\text{jet}}| < 2.4$ .

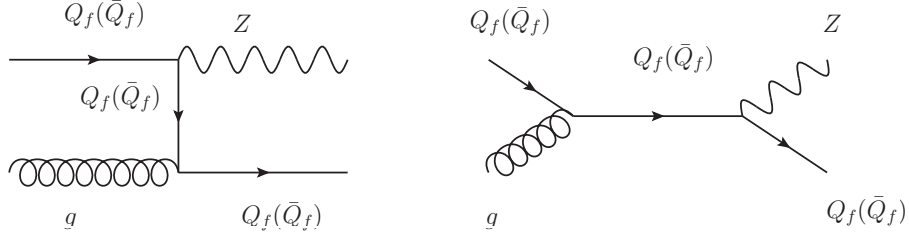


Figure 24: LO Feynman diagrams for the process  $Q_f(\bar{Q}_f)g \rightarrow ZQ_f(\bar{Q}_f)$ , where  $Q_f = c, b$ .

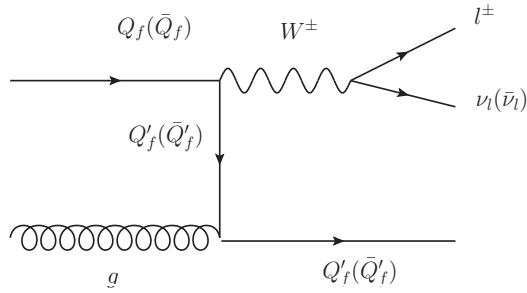


Figure 25: Example of an LO Feynman diagram for the process  $Q_f(\bar{Q}_f)g \rightarrow W^\pm Q'_f(\bar{Q}'_f)$ , where  $Q_f = c, b$  and  $Q'_f = b, c$  respectively.

which could give us information not only on the IC contribution but also on the IS in the proton.

At NLO in QCD,  $W/Z + Q_f$  diagrams, often more complicated than the ones presented in Figs. 24 and 25, must also be considered. As can be seen in Fig. 26, the heavy flavor jets in the final state of these diagrams come from a gluon splitting somewhere along the event chain, and does thus not feature any intrinsic quark contribution. If the cross-sections of these diagrams is large enough, the conclusions about the sensitivity of a measurement to intrinsic charm at the LHC will be affected. It is thus important to consider QCD NLO calculations in the current study.

To this end, we calculated the  $p_T$ -spectra of heavy flavor jets ( $b$  and  $c$ ) in association with a vector boson produced at NLO in  $pp$  collisions at  $\sqrt{s} = 8$  TeV/ $c$  using the parton level Monte Carlo (MC) generator MCFM version

6.7 [86]. The NLO corrections include the splitting of a gluon into a pair of heavy flavor quarks, and thus provides a better description of such process than what is yielded by parton showers, at least for the first splitting. The lack of further parton radiation and of hadronization in MCFM will affect the shape of the hadronic recoil to vector bosons and the  $p_T$  spectra of the leading heavy flavor jet in the various  $V + c$  and  $V + b$  ( $V = W$  or  $Z$ ) events, but it affects the predictions with and without an intrinsic charm contributions to the PDF in the exact same way. Conclusions that will be derived from MCFM about the IC sensitivity studies to be presented below are thus not affected by the fact that MCFM provides only a fixed order calculation with no parton shower or further non-perturbative corrections. For the various processes considered, the vector boson is required to decay leptonically, in order to allow experimental studies to trigger on these events, and the pseudo-rapidity of the heavy quark jet is required to satisfy  $|\eta_Q| < 1.5$ , to probe high- $x$  PDFs.

By selecting  $Z + c$ -jet events, where the  $c$ -jet is required to be rather forward ( $1.5 < |y_c| < 2.0$ ), we can see on the top panel of Fig. 27 that the  $c$ -jet transverse momentum spectrum of events with a 3.5 % intrinsic charm contribution to the PDF (CTEQ66c) features an excess, increasing with the  $c$ -jet  $p_T$ , compared to the corresponding differential cross-section when only extrinsic heavy flavor components of the PDF are considered (CTEQ66). These differential cross-section distributions have been obtained at NLO from the MCFM processes number 262. From the right panel of the same figure, showing the ratio of the two spectra obtained with and without an IC contribution, we can see that the excess in the  $c$ -jet  $p_T$  spectrum due to IC is of  $\sim 5$  % for  $p_T$  of 50 GeV/ $c$ , and rises to about 220 % for  $p_T \sim 300$  GeV/ $c$ . This effect can thus be observed at the LHC if the  $c$ -jet  $p_T$  differential cross-section in  $Z + c$  events can be measured with sufficient precision.

In the case of the  $W$  production in association with heavy flavor jets, the intrinsic charm contribution would be observed in a  $W + b$ -jet final state due to the change of flavor in the charged current. In MCFM, the NLO  $W + b$  Feynman diagrams for which the LO part is depicted in Fig. 25, correspond to the MCFM

processes 12 and 17 [86]. They provide the contribution to  $W + Q'$  which is sensitive to IC. The  $p_T$  spectrum of the  $b$ -jet is presented, for the sum of these processes, in Fig. 28 (top), where one calculation (squares) has been obtained at NLO in QCD with the CTEQ66c PDF that includes an IC contribution (about 3.5 %), and the other calculation (triangles) uses the CTEQ66 PDF, which does not include IC. On the bottom panel of Fig. 28, the ratio of these two spectra (with and without an IC contribution to the PDF used in the  $W + b$  production calculations) is presented. From this figure, one can see that the inclusion of the IC contribution to the PDF leads to an increase in the  $b$ -jet spectrum by a factor of about 1.9 at  $p_T > 250$  GeV/c. This is comparable to what was observed in the  $Z + c$  case of Fig. 27.

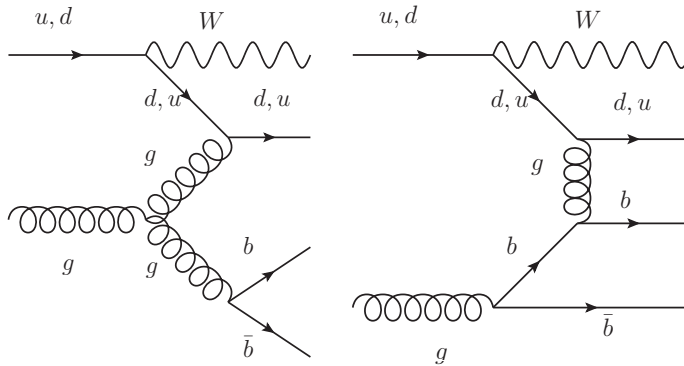


Figure 26: Some NLO Feynman diagrams for the process  $Q_f(\bar{Q}_f)g \rightarrow W^\pm Q'_f(\bar{Q}'_f)$ , where  $Q_f = c, b$  and  $Q'_f = b, c$  respectively. Left: gluon-splitting; Right:  $t$ -channel type of  $W$ -scattering with one gluon exchange in the intermediate state.

Similarly, the  $W + c$  final state would be sensitive to intrinsic strange while the  $Z + b$  final state would be sensitive to intrinsic bottom. These processes are however suboptimal for finding intrinsic quarks at the LHC. As mentioned above, the contribution of the IB to the PDF is suppressed by a factor of  $(\frac{m_c}{m_b})^2$  and is thus subdominant compared to intrinsic charm. The contribution of the intrinsic strangeness (IS) can be of the same order of magnitude as the IC according to [68, 81]. The  $Q^2$  evolution for this component has however not

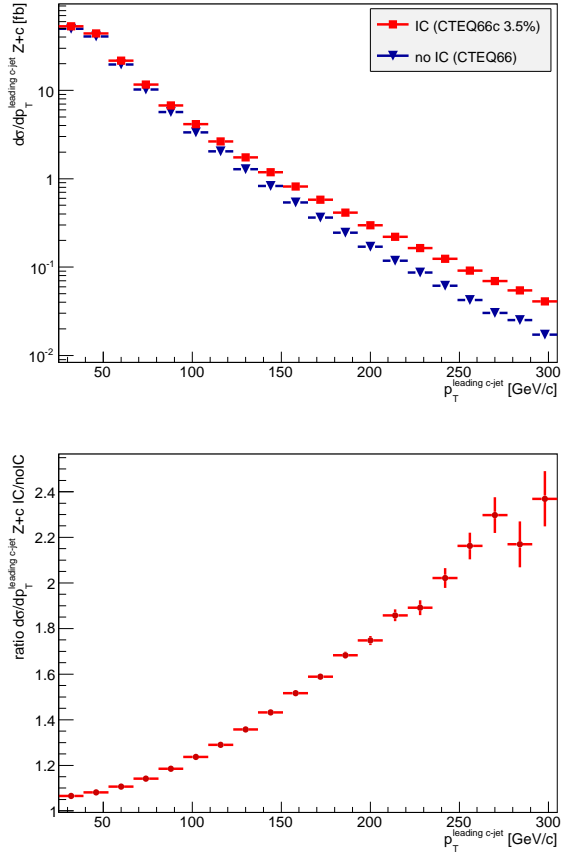


Figure 27: Comparison of the  $p_T$ -spectra for the NLO  $pp \rightarrow Z + c$  process 262 [86] obtained with PDF including an intrinsic charm component (CTEQ66c) and PDF having only an extrinsic component (CTEQ66) (top). Ratio of these two spectra (bottom).

been calculated up to now, and thus contains many unknowns. This is why this paper concentrate on the intrinsic charm component of the proton.

The above results of Figs. 27 and 28 seem a priori very encouraging regarding the capacity of the LHC to provide an observation of an intrinsic charm contribution to the PDFs in  $W/Z + Q_f$  events, but the real situation is unfortunately more complex than this. The  $W$  boson plus one or more  $b$ -quark jets production, calculated at NLO in the 4-flavor scheme (4FNS), for which two of the diagrams are represented in Fig. 26 must also be included. These

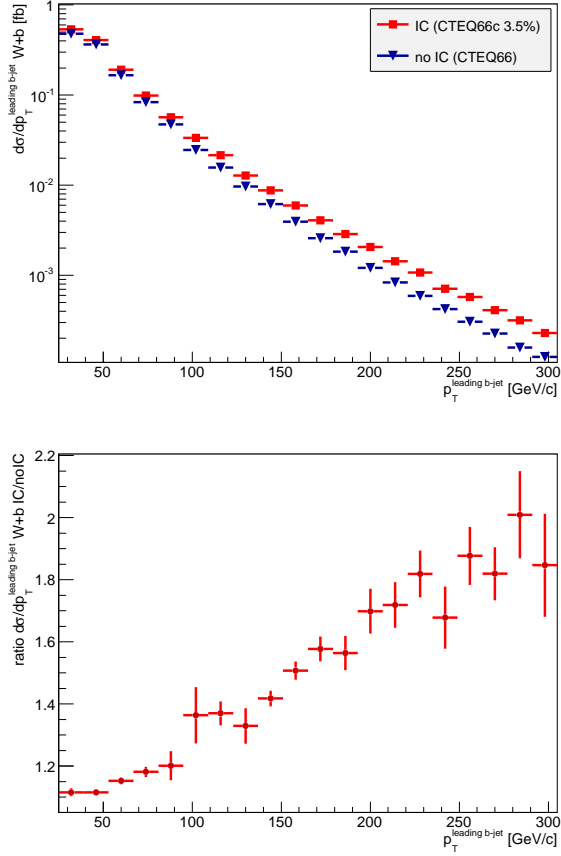


Figure 28: Comparison of the  $p_T$ -spectra for the NLO  $pp \rightarrow W + b$ , processes 12 + 17 [86] obtained with PDF including an intrinsic charm component (CTEQ66c) and PDF having only an extrinsic component (CTEQ66) (top). Ratio of these two spectra (bottom).

correspond to the MCFM processes number 401/406 and 402/407 [86]. Their total cross-section is about 50 times larger than the  $W + b$  processes sensitive to IC. As a result, the total  $W + b$  production is not sensitive to an intrinsic charm component of the PDF, as it was shown in [39], where the sum of all processes contributing to  $W + b$  has been taken into account. Fortunately the  $Z + c$  processes do not suffer from a similar large dilution of the intrinsic quark component because the  $Q_f + g \rightarrow Z + Q_f$  processes, which are sensitive to IC, are not Cabibbo-suppressed.

Another difficulty lies in the experimental identification of heavy flavor jets in the way how to select them, for example,  $Z + c$ -jet events in a very large  $Z$ -jets sample. Algorithms typically disentangling heavy flavor jets from light-quark jets exploit the longer lifetime of heavy-quark hadrons that decay away from the primary vertex of the main process, but close enough to allow for a reconstruction of the tracks of the decay products of the heavy-flavor hadron in the inner part of the detector. Such algorithms are typically not capable of explicitly distinguishing  $c$ -jets from  $b$ -jets; only the efficiency for identifying the heavy flavor nature of the jet would differ between  $c$ -jets and  $b$ -jets. For example, one of the ATLAS heavy-flavor tagging algorithm (MV1) yields an efficiency of 85 % for  $b$ -jet identification and 50 % for  $c$ -jet (for a working point where the light flavor rejection is 10), see References in [39]. As a result of such heavy flavor jet tagging algorithm, the selected  $Z + Q$  final state will be a mixture of  $Z + c$  and  $Z + b$ .

A priori, one would expect that  $Z + b$  events are sensitive to intrinsic bottom and therefore act only as a small background to intrinsic charm studies, when the two processes cannot be experimentally distinguished. The situation is however more complicated than this. Because of sum rules, an intrinsic charm component would affect the total  $b$ -quark contribution to the proton, and the  $Z + b$ -jet final state therefore becomes sensitive to intrinsic charm as well. As was shown in [39], this contribution is in the opposite direction of the intrinsic charm effect on  $Z + c$  processes presented in Fig. 27. In addition, the heavy flavor tagging efficiency is lower for  $c$ -jets than it is for  $b$ -jets, therefore increasing the weight of the negative  $Z + b$  contribution to the total  $Z$  plus heavy flavor tagged jets signal. The question is thus: are  $Z + Q$ -jet events still sensitive to intrinsic charm?

To avoid these difficulties in [39] the following idea to search the IC signal in the  $Z/W$  boson production accompanied by heavy flavor jets was suggested. The new idea is to use the ratio of the leading heavy flavor spectra in inclusive heavy flavor  $Z + Q$  to  $W + Q$  events to verify the predictions about an IC contribution to the proton. The background related to the  $Z/W$  production with

association of light jets is included, which does not change the main conclusion on the IC signal in that ratio. We would like to stress also that studying the ratios discussed above we avoid many uncertainties related to a background due to the light jet production, rescaling in QCD and many others because they are almost cancelled. Such measurements can already be made with ATLAS and CMS available data.

To verify this, the ratio of the  $p_T$  spectra of the leading heavy flavor jet ( $b$ ,  $c$ ) produced in  $Zb + Zc$  and  $Wb + Wc + Wbj$  processes has been to the proton. The of the calculation is presented in Fig. 29. As can be seen in this figure, the sensitivity to IC signal observed in  $Z + Q$  is maintained in the ratio, which can amount to about 160 % of the extrinsic only contribution at  $p_T$  of about 270 – 300 GeV/ $c$ . This ratio measurement would, at least partially, cancel a number of large experimental systematic uncertainties, especially since in our proposal,  $V + c$ -jets and  $V + b$ -jets are both considered as signal and not treated as a background with respect to the other. This would allow for a clear signal at the LHC, if the IC contribution is sufficiently high (here we considered a 3.5 % contribution). In the case where no excess is observed, limits on the IC contribution to the proton can be obtained from such measurement. Note that ratio predictions obtained with MCFM [39] would agree with predictions that include a parton shower and a modeling of the hadronization, because such effects cancel in the ratio for jets above  $\sim 100$  GeV/ $c$ .

As discussed above, a high  $p_T$  and relatively high rapidity heavy-flavor jet enhances the probability to have a heavy flavor quark in the initial state with a high- $x$  fraction, ensuring that the effect of intrinsic quarks on the cross-section is more prominent. This is the reason why we proposed to measure the ratio of  $Z + Q$  to  $W + Q$  differential cross-sections as a function of the transverse momentum of the leading heavy-flavor jet measured within a specific rapidity interval. As indicated by Eq. 20, a large- $x$  heavy flavor quark will in general be achieved by a high-value of the Feynman variable  $x_F^V$  of the final state vector boson  $V$  recoiling to the hadronic system. While such variable cannot be reconstructed at the detector level in  $W + Q$  events because of the presence of an undetectable

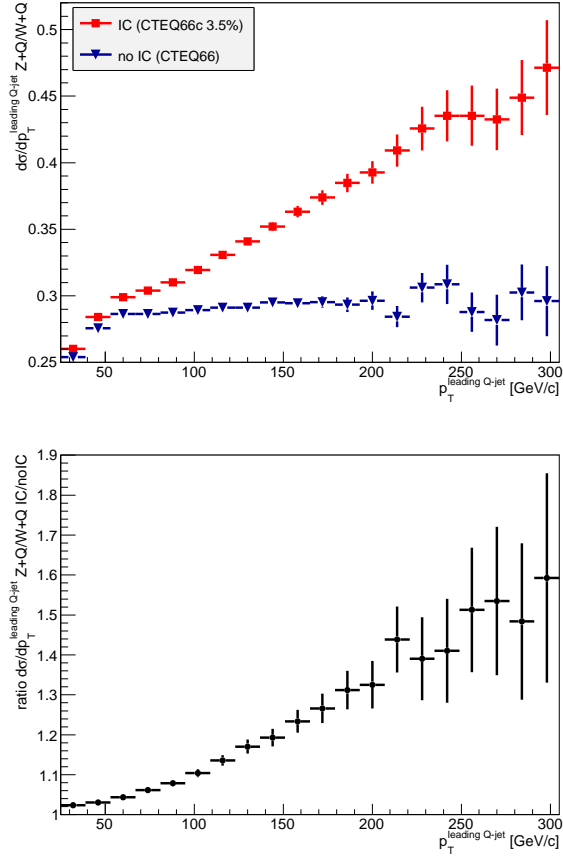


Figure 29: Comparison of the ratio of the  $p_T$ -spectra for the  $Z + Q$  to  $W + Q$  NLO processes obtained with PDF including an intrinsic charm component (CTEQ66c) and PDF having only an extrinsic component (CTEQ66). Heavy flavor jet tagging efficiencies have been applied to the  $c$ -jets and the  $b$ -jets (top). Ratio of these two ratios of spectra (bottom).

neutrino in the final state, it is possible to construct a quantity highly correlated to such Feynman variable by using the leading heavy-flavor jet in the final state, rather than the vector boson. We therefore propose to investigate the sensitivity to IC of the ratio of the  $Z + Q$  to  $W + Q$  differential cross-sections as a function of the pseudo-Feynman variable of the leading heavy-flavor jet defined as:

$$x_F^Q = \frac{2p_T^{\text{Lead } Q\text{-jet}}}{\sqrt{s}} \sinh(\eta_Q), \quad (24)$$

where  $p_T^{\text{Lead } Q\text{-jet}}$  is the transverse momentum of the leading heavy flavor jet in the final state and  $\eta_Q$  is the pseudo-rapidity of this jet.

First, the sensitivity of  $Z + Q$  events to intrinsic charm is presented in the top panel of Fig. 30 as a function of this pseudo-Feynman variable of the leading heavy-flavor jet. The  $x_F^Q$ -spectrum has been obtained from the total NLO  $pp \rightarrow Z + b(\bar{b})$  plus  $pp \rightarrow Z + c(\bar{c})$  contributions calculated with MCFM (processes 261, 262 [86]) for collisions at  $\sqrt{s} = 8 \text{ TeV}/c$ . The distribution displayed with red square has been obtained using the CTEQ66c PDF distribution displayed with red square has been obtained using the CTEQ66c PDF that includes an intrinsic charm component, while the distribution displayed as blue inverted triangles have been obtained with the CTEQ66 PDF that only contains an extrinsic charm component. In the bottom panel the ratio of the two spectra is shown.

Fig. 31 presents the sensitivity to an intrinsic charm component to the PDF for the ratio of  $Z + Q$  to  $W + Q$  events as a function of the pseudo-Feynman variable  $x_F^Q$ . In this figure, heavy flavor tagging has been applied to both  $Z + Q$  and  $W + Q$  processes. An IC contribution of 3.5 % yields a change by a factor of 2 to 4 in the  $Z + Q$  to  $W + Q$  cross-section ratio at  $x_F^Q \simeq 0.3 - 0.4$  compared to the calculation where the PDF do not include any IC component. The number of events in that kinematic region runs from about a few hundred up to a few thousand events, for both  $Z + Q$  and  $W + Q$  processes. This results in a reduced statistical uncertainty on the  $Z + Q$  to  $W + Q$  ratio compared to the proposed ratio measured as a function of the transverse momentum of the leading heavy flavor jet in the phase space region discussed above. Because the pseudo-Feynman variable and the  $Q$ -jet transverse momentum observables correspond to significantly different distributions in shape, both sensitive to an intrinsic charm contribution to the proton, but with different sensitivity to the various systematic uncertainties, we thus have here two complementary ratio observables to be measured at the LHC in order to observed an IC contribution to the proton, or determine an upper limit on it.

As discussed above, the leading heavy flavor jet transverse momentum and

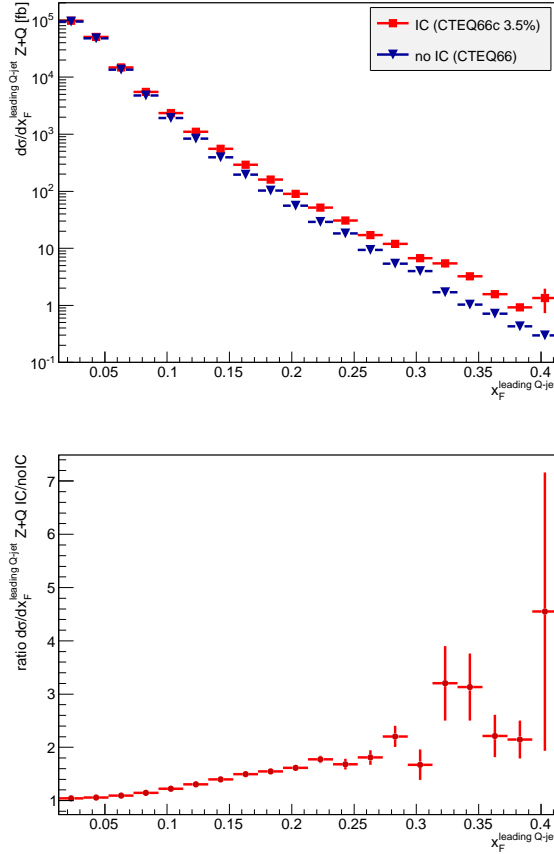


Figure 30: Comparison of the  $x_F^Q$ -spectra for the total NLO  $pp \rightarrow Z + b(\bar{b})$  process plus  $pp \rightarrow Z + c(\bar{c})$  (processes 261, 262 [86]) obtained with PDF including an intrinsic charm component (CTEQ66c) and PDF having only an extrinsic component (CTEQ66) (top). Ratio of these two spectra (bottom).

rapidity distributions are similar for  $b$ -jet and  $c$ -jet in  $Z + Q$  and  $W + Q$  events. As a consequence, the experimental uncertainties on  $Q$ -jet energy measurements and heavy flavor tagging efficiencies will get significantly reduced in the ratio measurements proposed above. The Feynman diagrams contributing to  $Z + Q$  and  $W + Q$  processes are however quite different. It is therefore important to verify that a similar cancellation of the theory uncertainty also occurs in this ratio, therefore not impeding the conclusion about IC that can be obtained with

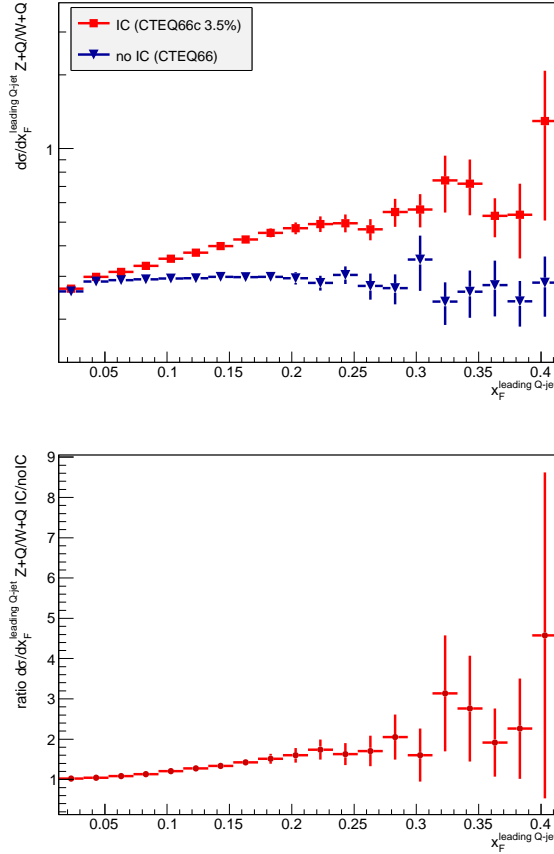


Figure 31: Comparison of the ratio of the  $x_F^Q$ -spectra for the  $Z + Q$  to  $W + Q$  NLO processes obtained with PDF including an intrinsic charm component (CTEQ66c) and PDF having only an extrinsic component (CTEQ66) (top). Ratio of these two ratios of spectra (bottom).

such ratio. The dominant theoretical systematic uncertainty on a NLO cross-section calculation obtained at fixed order in perturbative QCD comes, by far, from the uncertainty introduced by the choice of renormalization ( $\mu_R$ ) and factorization ( $\mu_F$ ) scales in the calculation. In the current calculations performed with MCFM [86], the central predictions were obtained with a dynamic scale  $\mu_R = \mu_F = H_T$ , where  $H_T$  is the scalar sum of the transverse momentum of all the particles ( $p_{T_i}$ ) in the final state ( $H_T = \sum_i^n p_{T_i}$ ). In order to assess the

sensitivity of the calculations to this choice of scale, cross-sections have been calculated with two other choices of scale,  $H_T \cdot 2$  and  $H_T/2$ , and results compared to the nominal predictions.

It was shown in [39] that the choice of scale made in both predictions is the same, therefore leaving a ratio of predictions with IC to predictions without IC independent of the choice of scale.

## 7. Conclusion

The quark and gluon distribution functions of the proton encode the color-confining dynamics of QCD. These probability distributions are directly related to the frame-independent light-front wavefunctions, the eigensolutions of the QCD Hamiltonian. Because of QCD factorization, the PDFs allow the computation of the cross sections for virtually all high energy collision processes studied at the LHC. However, the heavy quark contribution to the proton PDFs is still a major uncertainty. As we have discussed, QCD predicts two sources of heavy quarks to the constituent structure of the light hadrons – the standard small- $x$  extrinsic contribution at from gluon splitting  $g \rightarrow Q\bar{Q}$  – plus the intrinsic contribution at large  $x$  which arises from diagrams where the  $Q\bar{Q}$  pair is connected by two or more gluons to the valence quarks. The maximum configuration of such intrinsic contributions occur at minimal off-shellness; i.e., when all of the quarks in the  $|uudQ\bar{Q}\rangle$  Fock state are at rest in the proton’s rest frame, corresponding to equal rapidity  $y_i$  in the moving proton, and thus where the momentum fraction carried by each quark is proportional to its transverse mass:  $x_i \propto \sqrt{m_{Ti}^2 + \vec{k}_{Ti}^2}$ .

The hypothesis of *intrinsic* quark components in the proton at high  $x$  was originally suggested in [6] was motivated possible explanation of the large cross-section for the forward open charm production in  $pp$  collision at ISR energies [7–10]. However, the accuracy of the experimental data on the open charm production at large  $x$  does not provide precise constraints on the intrinsic heavy quark probability. We have discussed a number of experiments such as as deep inelas-

tic scattering measurements of  $c(c, Q)$  at the EMC and HERA; soft processes of the open charm or strangeness production and even the Higgs boson production in  $pp$  collisions at LHC. We have also shown that the inclusive production of open charm or strangeness at high transverse momentum can serve as a tool for the search for the heavy quark  $Q\bar{Q}$  Fock states in the nucleon. The IC or IS signal can be visible in the  $p_T$ -spectrum of  $D$ -mesons or  $K$ -mesons produced, for example, in  $pp$  collisions at their large rapidities  $y$  and transverse momenta  $p_T$ . It can be verified at CERN experiments such as the LHC and NA61.

The semi-inclusive production of prompt photons or gauge vector bosons in association with heavy flavor jets  $c$  or  $b$  provides an ideal method for verifying the IC contribution in the proton PDF. The increase of  $p_T$  spectrum of these hadrons or jets produced at large  $p_T$  and the forward rapidity region of ATLAS or CMS ( $1.5 < |y| < 2.4$ ) due to the IC enhancement in the PDF is predicted. We also have found observables very sensitive to the non-zero intrinsic charm contribution to the proton density. They are the  $\gamma/Z + b$  production. These ratios should be decreasing in the absence of the IC contribution to the PDF and they should be flat or increasing if the IC is included, when  $p_T$  grows. This prediction, can also verify the IC hypothesis at LHC.

We argued that the ratio of the cross-sections  $\gamma/Z + c$  and  $\gamma/Z + b$  integrated over  $p_T > p_T^{\min}$  with  $p_T^{\min} \geq 100$  GeV/c can be used to determine the IC probability  $w$  from the future LHC data because we calculated it as a function of  $w$ . The advantage of the proposed ratios is that the theoretical uncertainties are very small, while the uncertainties for the  $p_T$ -spectra of photons or  $Z$  bosons produced in association with the  $c$  or  $b$  jets are large. Therefore, the search for the IC signal by analyzing the ratio  $\sigma(\gamma/Z + c)/\sigma(\gamma/Z + b)$  can be more promising.

We have also shown that because of dominance of gluon-splitting processes, the production of  $W$ -bosons accompanied by heavy flavor jets is not directly sensitive to intrinsic heavy quarks. However, we can take advantage of this fact to propose a promising new method which reduces the expected systematic uncertainties by comparing the differential cross-section for  $W$  plus heavy flavor

jets to that in  $Z + Q$  events. The ratio of the leading heavy flavor spectra in inclusive heavy flavor  $Z + Q$  to  $W + Q$  events can thus be used to determine the intrinsic heavy quark contribution to the proton PDF. Such measurements can already be made with available data from ATLAS and CMS.

We have also discussed the fact that the existence of intrinsic heavy charm and bottom quarks in the proton wavefunction implies that the Higgs boson will be produced at high momentum fractions  $x_F > 0.8$  in  $pp \rightarrow HX$  collisions at the LHC, via the same mechanism that produces quarkonium states such as  $pp \rightarrow J/\psi X$  at high  $x_F$ . In addition, we have noted that fixed target experiments at the LHC such as the AFTER facility and the SMOG nuclear target at LHCb can materialize the intrinsic heavy quark Fock states in a novel way. Since the momentum distributions of the intrinsic heavy quarks in the  $|uudQ\bar{Q}\rangle$  Fock state are maximal when all of the constituents have the same rapidity, the collision of the LHC proton beam with nucleons in the nuclear target will lead to the production of heavy hadrons such as the  $\Lambda_b$  and exotic heavy quark states, such as tetraquarks and pentaquarks, at *small rapidities* relative to the rapidity of the target. Each of these novel processes will illuminate one of the most interesting features of QCD bound state dynamics – intrinsic heavy quarks.

## 8. Acknowledgements

We thank A. Glazov for extremely helpful discussions and recommendations for the predictions on the search for the possible intrinsic heavy flavor components in  $pp$  collisions at high energies. We are also grateful to P-H. Beauchmin, T. Dado, M. Demichev, N. Husseyonov, A.V. Lipatov, T. Stavreva, Yu. Stepanenko and M. Stockton for very productive collaboration, H. Jung, R. Keys, B.Z. Kopeliovich, A. Likhoded, S. Prince, S. Rostami, L. Rottoli, O.V. Teryaev and M. Williams for very helpful discussions. This research was supported in part by the Department of Energy contract DE-AC02-76SF00515 SLAC-PUB-16844.

## 9. References

### References

- [1] V. N. Gribov, L. N. Lipatov, *Sov. J. Nucl. Phys.* 15 (1972) 438–450. [*Yad. Fiz.*15,781(1972)].
- [2] G. Altarelli, G. Parisi, *Nucl. Phys.* B126 (1977) 298. doi:10.1016/0550-3213(77)90384-4.
- [3] Y. L. Dokshitzer, *Sov. Phys. JETP* 46 (1977) 641–653. [*Zh. Eksp. Teor. Fiz.*73,1216(1977)].
- [4] S. J. Brodsky, J. C. Collins, S. D. Ellis, J. F. Gunion, A. H. Mueller, in: ELECTROWEAK SYMMETRY BREAKING. PROCEEDINGS, WORKSHOP, BERKELEY, USA, JUNE 3-22, 1984. URL: <http://www-public.slac.stanford.edu/sciDoc/docMeta.aspx?slacPubNumber=SLAC-PUB-15471>.
- [5] M. Franz, M. V. Polyakov, K. Goeke, *Phys. Rev.* D62 (2000) 074024. doi:10.1103/PhysRevD.62.074024. arXiv:hep-ph/0002240.
- [6] S. J. Brodsky, P. Hoyer, C. Peterson, N. Sakai, *Phys. Lett.* B93 (1980) 451–455. doi:10.1016/0370-2693(80)90364-0.
- [7] D. Drijard, et al. (CERN-College de France-Heidelberg-Karlsruhe), *Phys. Lett.* B81 (1979) 250–254. doi:10.1016/0370-2693(79)90535-5.
- [8] K. L. Giboni, et al., *Phys. Lett.* B85 (1979) 437–442. doi:10.1016/0370-2693(79)91291-7.
- [9] W. S. Lockman, T. Meyer, J. Rander, P. Schlein, R. Webb, S. Erhan, J. Zsembery, *Phys. Lett.* B85 (1979) 443–446. doi:10.1016/0370-2693(79)91292-9.
- [10] D. Drijard, et al. (ACCDHW), *Phys. Lett.* B85 (1979) 452–457. doi:10.1016/0370-2693(79)91294-2.

- [11] R. Laha, S. J. Brodsky (2016). [arXiv:1607.08240](#).
- [12] A. Aktas, et al. (H1), *Eur. Phys. J. C* 45 (2006) 23–33. doi:10.1140/epjc/s2005-02415-6. [arXiv:hep-ex/0507081](#).
- [13] S. J. Brodsky, C. Peterson, N. Sakai, *Phys. Rev. D* 23 (1981) 2745. doi:10.1103/PhysRevD.23.2745.
- [14] S. J. Brodsky, *Few Body Syst.* 36 (2005) 35–52. doi:10.1007/s00601-004-0077-8. [arXiv:hep-ph/0411056](#).
- [15] S. J. Brodsky, A. Kusina, F. Lyonnet, I. Schienbein, H. Spiesberger, R. Vogt, *Adv. High Energy Phys.* 2015 (2015) 231547. doi:10.1155/2015/231547. [arXiv:1504.06287](#).
- [16] J. Pumplin, *Phys. Rev. D* 73 (2006) 114015. doi:10.1103/PhysRevD.73.114015. [arXiv:hep-ph/0508184](#).
- [17] J. J. Aubert, et al. (European Muon), *Nucl. Phys. B* 213 (1983) 31–64. doi:10.1016/0550-3213(83)90174-8.
- [18] R. D. Ball, V. Bertone, M. Bonvini, S. Carrazza, S. Forte, A. Guffanti, N. P. Hartland, J. Rojo, L. Rottoli (NNPDF) (2016). [arXiv:1605.06515](#).
- [19] R. D. Ball, et al. (NNPDF), *JHEP* 04 (2015) 040. doi:10.1007/JHEP04(2015)040. [arXiv:1410.8849](#).
- [20] S. Dulat, T.-J. Hou, J. Gao, M. Guzzi, J. Huston, P. Nadolsky, J. Pumplin, C. Schmidt, D. Stump, C. P. Yuan, *Phys. Rev. D* 93 (2016) 033006. doi:10.1103/PhysRevD.93.033006. [arXiv:1506.07443](#).
- [21] M. Adamovich, et al. (WA82), *Phys. Lett. B* 305 (1993) 402–406. doi:10.1016/0370-2693(93)91074-W.
- [22] G. A. Alves, et al. (E769), *Phys. Rev. Lett.* 72 (1994) 812–815. doi:10.1103/PhysRevLett.72.812, [Erratum: *Phys. Rev. Lett.* 72,1946(1994)].

- [23] E. M. Aitala, et al. (E791), Phys. Lett. B371 (1996) 157–162. doi:10.1016/0370-2693(96)00093-7. arXiv:hep-ex/9601001.
- [24] A. B. Kaidalov, Phys. Lett. B116 (1982) 459–463. doi:10.1016/0370-2693(82)90168-X.
- [25] A. Capella, U. Sukhatme, C.-I. Tan, J. Tran Thanh Van, Phys. Rept. 236 (1994) 225–329. doi:10.1016/0370-1573(94)90064-7.
- [26] A. B. Kaidalov, O. I. Piskunova, Z. Phys. C30 (1986) 145. doi:10.1007/BF01560688.
- [27] Yu. M. Shabelski, Surveys High Energ. Phys. 9 (1995) 1–88. doi:10.1080/01422419508225681.
- [28] G. I. Lykasov, G. H. Arakelian, M. N. Sergeenko, Phys. Part. Nucl. 30 (1999) 343–368. doi:10.1134/1.953111, [Fiz. Elem. Chast. Atom. Yadra30,817(1999)].
- [29] S. Barlag, et al. (ACCMOR), Phys. Lett. B247 (1990) 113–120. doi:10.1016/0370-2693(90)91058-J.
- [30] G. Bari, et al., Nuovo Cim. A104 (1991) 571–599. doi:10.1007/BF02813593.
- [31] V. M. Abazov, et al. (D0), Phys. Rev. Lett. 102 (2009) 192002. doi:10.1103/PhysRevLett.102.192002. arXiv:0901.0739.
- [32] V. M. Abazov, et al. (D0), Phys. Lett. B714 (2012) 32–39. doi:10.1016/j.physletb.2012.06.056. arXiv:1203.5865.
- [33] V. M. Abazov, et al. (D0), Phys. Lett. B719 (2013) 354–361. doi:10.1016/j.physletb.2013.01.033. arXiv:1210.5033.
- [34] T. Aaltonen, et al. (CDF), Phys. Rev. D81 (2010) 052006. doi:10.1103/PhysRevD.81.052006. arXiv:0912.3453.

- [35] T. Aaltonen, et al. (CDF), Phys. Rev. Lett. 111 (2013) 042003. doi:10.1103/PhysRevLett.111.042003. arXiv:1303.6136.
- [36] M. V. Polyakov, A. Schafer, O. V. Teryaev, Phys. Rev. D60 (1999) 051502. doi:10.1103/PhysRevD.60.051502. arXiv:hep-ph/9812393.
- [37] T. P. Stavreva, J. F. Owens, Phys. Rev. D79 (2009) 054017. doi:10.1103/PhysRevD.79.054017. arXiv:0901.3791.
- [38] V. A. Bednyakov, M. A. Demichev, G. I. Lykasov, T. Stavreva, M. Stockton, Phys. Lett. B728 (2014) 602–606. doi:10.1016/j.physletb.2013.12.031. arXiv:1305.3548.
- [39] P.-H. Beauchemin, V. A. Bednyakov, G. I. Lykasov, Yu. Yu. Stepanenko, Phys. Rev. D92 (2015) 034014. doi:10.1103/PhysRevD.92.034014. arXiv:1410.2616.
- [40] A. V. Lipatov, G. I. Lykasov, Yu. Yu. Stepanenko, V. A. Bednyakov, Phys. Rev. D94 (2016) 053011. doi:10.1103/PhysRevD.94.053011. arXiv:1606.04882.
- [41] S. J. Brodsky, B. Kopeliovich, I. Schmidt, J. Soffer, Phys. Rev. D73 (2006) 113005. doi:10.1103/PhysRevD.73.113005. arXiv:hep-ph/0603238.
- [42] S. J. Brodsky, A. S. Goldhaber, B. Z. Kopeliovich, I. Schmidt, Nucl. Phys. B807 (2009) 334–347. doi:10.1016/j.nuclphysb.2008.09.014. arXiv:0707.4658.
- [43] S. J. Brodsky, F. Fleuret, C. Hadjidakis, J. P. Lansberg, Phys. Rept. 522 (2013) 239–255. doi:10.1016/j.physrep.2012.10.001. arXiv:1202.6585.
- [44] J. W. Negele, et al., Nucl. Phys. Proc. Suppl. 128 (2004) 170–178. doi:10.1016/S0920-5632(03)02474-5. arXiv:hep-lat/0404005, [,170(2004)].
- [45] W. Schroers, Nucl. Phys. A755 (2005) 333–336. doi:10.1016/j.nuclphysa.2005.03.034. arXiv:hep-ph/0501156.

- [46] J. Pumplin, D. R. Stump, J. Huston, H. L. Lai, P. M. Nadolsky, W. K. Tung, JHEP 07 (2002) 012. doi:10.1088/1126-6708/2002/07/012. arXiv:hep-ph/0201195.
- [47] D. Stump, J. Huston, J. Pumplin, W.-K. Tung, H. L. Lai, S. Kuhlmann, J. F. Owens, JHEP 10 (2003) 046. doi:10.1088/1126-6708/2003/10/046. arXiv:hep-ph/0303013.
- [48] R. S. Thorne, A. D. Martin, W. J. Stirling, R. G. Roberts, in: Deep inelastic scattering. Proceedings, 12th International Workshop, DIS 2004, Strbske Pleso, Slovakia, April 14-18, 2004. Vol. 1 + 2, pp. 427-432. URL: <http://www.saske.sk/dis04/proceedings/A/thorne.ps.gz>. arXiv:hep-ph/0407311.
- [49] S. J. Brodsky, B.-Q. Ma, Phys. Lett. B381 (1996) 317-324. doi:10.1016/0370-2693(96)00597-7. arXiv:hep-ph/9604393.
- [50] J. Pumplin, H. L. Lai, W. K. Tung, Phys. Rev. D75 (2007) 054029. doi:10.1103/PhysRevD.75.054029. arXiv:hep-ph/0701220.
- [51] J. F. Donoghue, E. Golowich, Phys. Rev. D15 (1977) 3421. doi:10.1103/PhysRevD.15.3421.
- [52] S. Paiva, M. Nielsen, F. S. Navarra, F. O. Duraes, L. L. Barz, Mod. Phys. Lett. A13 (1998) 2715-2724. doi:10.1142/S0217732398002886. arXiv:hep-ph/9610310.
- [53] W. Melnitchouk, A. W. Thomas, Phys. Lett. B414 (1997) 134-139. doi:10.1016/S0370-2693(97)01150-7. arXiv:hep-ph/9707387.
- [54] F. M. Steffens, W. Melnitchouk, A. W. Thomas, Eur. Phys. J. C11 (1999) 673-683. doi:10.1007/s100529900189, 10.1007/s100520050663. arXiv:hep-ph/9903441.
- [55] T. J. Hobbs, J. T. Londergan, W. Melnitchouk, Phys. Rev. D89 (2014) 074008. doi:10.1103/PhysRevD.89.074008. arXiv:1311.1578.

- [56] P. M. Nadolsky, H.-L. Lai, Q.-H. Cao, J. Huston, J. Pumplin, D. Stump, W.-K. Tung, C. P. Yuan, Phys. Rev. D78 (2008) 013004. doi:10.1103/PhysRevD.78.013004. arXiv:0802.0007.
- [57] S. J. Brodsky, S. Gardner, Phys. Rev. Lett. 116 (2016) 019101. doi:10.1103/PhysRevLett.116.019101. arXiv:1504.00969.
- [58] R. Ammar, et al. (LEBC-MPS), Phys. Lett. B183 (1987) 110. doi:10.1016/0370-2693(87)91427-4, [Erratum: Phys. Lett.B192,478(1987)].
- [59] J. Russ, et al. (SELEX), in: High-energy physics. Proceedings, 29th International Conference, ICHEP'98, Vancouver, Canada, July 23-29, 1998. Vol. 1, 2, pp. 1259–1262. URL: <http://alice.cern.ch/format/showfull?sysnb=0300703>. arXiv:hep-ex/9812031.
- [60] S. J. Brodsky, Nucl. Part. Phys. Proc. 258-259 (2015) 23–30. doi:10.1016/j.nuclphysbps.2015.01.007. arXiv:1410.0404.
- [61] J. Blmllein, Phys. Lett. B753 (2016) 619–621. doi:10.1016/j.physletb.2015.12.068. arXiv:1511.00229.
- [62] S. Catani, D. de Florian, G. Rodrigo, W. Vogelsang, Phys. Rev. Lett. 93 (2004) 152003. doi:10.1103/PhysRevLett.93.152003. arXiv:hep-ph/0404240.
- [63] F. G. Garcia, et al. (SELEX), Phys. Lett. B528 (2002) 49–57. doi:10.1016/S0370-2693(01)01484-8. arXiv:hep-ex/0109017.
- [64] S. Rostami, A. Khorramian, A. Aleedaneshvar, M. Goharipour, J. Phys. G43 (2016) 055001. doi:10.1088/0954-3899/43/5/055001. arXiv:1510.08421.
- [65] S. Catani, M. Ciafaloni, F. Hautmann, Nucl. Phys. B366 (1991) 135–188. doi:10.1016/0550-3213(91)90055-3.

- [66] G. I. Lykasov, V. A. Bednyakov, A. F. Pikelner, N. I. Zimine, *Europhys. Lett.* 99 (2012) 21002. doi:10.1209/0295-5075/99/21002. arXiv:1205.1131.
- [67] V. P. Goncalves, F. S. Navarra, *Nucl. Phys. A*842 (2010) 59–71. doi:10.1016/j.nuclphysa.2010.04.004. arXiv:0805.0810.
- [68] J.-C. Peng, W.-C. Chang, *PoS QNP2012* (2012) 012. arXiv:1207.2193.
- [69] A. Airapetian, et al. (HERMES), *Phys. Lett. B*666 (2008) 446–450. doi:10.1016/j.physletb.2008.07.090. arXiv:0803.2993.
- [70] V. A. Litvine, A. K. Likhoded, *Phys. Atom. Nucl.* 62 (1999) 679–692. [*Yad. Fiz.*62,728(1999)].
- [71] A. V. Lipatov, M. A. Malyshev, N. P. Zotov, *JHEP* 05 (2012) 104. doi:10.1007/JHEP05(2012)104. arXiv:1204.3828.
- [72] A. V. Lipatov, N. P. Zotov, *J. Phys. G*34 (2007) 219. doi:10.1088/0954-3899/34/2/005. arXiv:hep-ph/0507243.
- [73] R. Vogt, *Prog. Part. Nucl. Phys.* 45 (2000) S105–S169. doi:10.1016/S0146-6410(00)90012-7. arXiv:hep-ph/0011298.
- [74] F. S. Navarra, M. Nielsen, C. A. A. Nunes, M. Teixeira, *Phys. Rev. D*54 (1996) 842–846. doi:10.1103/PhysRevD.54.842. arXiv:hep-ph/9504388.
- [75] J. C. Collins, D. E. Soper, G. F. Sterman, *Adv. Ser. Direct. High Energy Phys.* 5 (1989) 1–91. doi:10.1142/9789814503266\_0001. arXiv:hep-ph/0409313.
- [76] R. P. Feynman, R. D. Field, G. C. Fox, *Phys. Rev. D*18 (1978) 3320. doi:10.1103/PhysRevD.18.3320.
- [77] V. A. Bednyakov, A. A. Grinyuk, G. I. Lykasov, M. Poghosyan, *Int. J. Mod. Phys. A*27 (2012) 1250042. doi:10.1142/S0217751X1250042X. arXiv:1104.0532.

- [78] B. A. Kniehl, G. Kramer, I. Schienbein, H. Spiesberger, *Eur. Phys. J. C* 72 (2012) 2082. doi:10.1140/epjc/s10052-012-2082-2. arXiv:1202.0439.
- [79] A. Airapetian, et al. (HERMES), *Phys. Rev. D* 89 (2014) 097101. doi:10.1103/PhysRevD.89.097101. arXiv:1312.7028.
- [80] D. de Florian, R. Sassot, M. Stratmann, *Phys. Rev. D* 75 (2007) 114010. doi:10.1103/PhysRevD.75.114010. arXiv:hep-ph/0703242.
- [81] G. I. Lykasov, I. V. Bednyakov, M. A. Demichev, Yu. Yu. Stepanenko, *Nucl. Phys. Proc. Suppl.* 245 (2013) 215–222. doi:10.1016/j.nuclphysbps.2013.10.042. arXiv:1309.3168.
- [82] S. Albino, B. A. Kniehl, G. Kramer, *Nucl. Phys. B* 803 (2008) 42–104. doi:10.1016/j.nuclphysb.2008.05.017. arXiv:0803.2768.
- [83] M. L. Mangano, *Phys. Usp.* 53 (2010) 109–132. doi:10.3367/UFNe.0180.201002a.0113, [*Usp. Fiz. Nauk*180,113(2010)].
- [84] L. Rottoli, in: *Proceedings, 24th International Workshop on Deep-Inelastic Scattering and Related Subjects (DIS 2016)*. URL: <https://inspirehep.net/record/1473188/files/arXiv:1606.09289.pdf>. arXiv:1606.09289.
- [85] R. Aaij, et al. (LHCb), *JINST* 9 (2014) P12005. doi:10.1088/1748-0221/9/12/P12005. arXiv:1410.0149.
- [86] J. M. Campbell, R. K. Ellis, *Phys. Rev. D* 65 (2002) 113007. doi:10.1103/PhysRevD.65.113007. arXiv:hep-ph/0202176.
- [87] E. M. Levin, M. G. Ryskin, Yu. M. Shabelski, A. G. Shuvaev, *Sov. J. Nucl. Phys.* 53 (1991) 657. [*Yad. Fiz.*53,1059(1991)].
- [88] L. V. Gribov, E. M. Levin, M. G. Ryskin, *Phys. Rept.* 100 (1983) 1–150. doi:10.1016/0370-1573(83)90022-4.

- [89] E. A. Kuraev, L. N. Lipatov, V. S. Fadin, Sov. Phys. JETP 44 (1976) 443–450. [Zh. Eksp. Teor. Fiz.71,840(1976)].
- [90] E. A. Kuraev, L. N. Lipatov, V. S. Fadin, Sov. Phys. JETP 45 (1977) 199–204. [Zh. Eksp. Teor. Fiz.72,377(1977)].
- [91] I. I. Balitsky, L. N. Lipatov, Sov. J. Nucl. Phys. 28 (1978) 822–829. [Yad. Fiz.28,1597(1978)].
- [92] B. Andersson, et al. (Small x), Eur. Phys. J. C25 (2002) 77–101. doi:10.1007/s10052-002-0998-7. arXiv:hep-ph/0204115.
- [93] J. R. Andersen, et al. (Small x), Eur. Phys. J. C35 (2004) 67–98. doi:10.1140/epjc/s2004-01775-7. arXiv:hep-ph/0312333.
- [94] J. R. Andersen, et al. (Small x), Eur. Phys. J. C48 (2006) 53–105. doi:10.1140/epjc/s2006-02615-6. arXiv:hep-ph/0604189.
- [95] L. N. Lipatov, M. I. Vyazovsky, Nucl. Phys. B597 (2001) 399–409. doi:10.1016/S0550-3213(00)00709-4. arXiv:hep-ph/0009340.
- [96] A. V. Bogdan, V. S. Fadin, Nucl. Phys. B740 (2006) 36–57. doi:10.1016/j.nuclphysb.2006.01.033. arXiv:hep-ph/0601117.
- [97] M. Hentschinski, A. Sabio Vera, Phys. Rev. D85 (2012) 056006. doi:10.1103/PhysRevD.85.056006. arXiv:1110.6741.
- [98] M. Hentschinski, Nucl. Phys. B859 (2012) 129–142. doi:10.1016/j.nuclphysb.2012.02.001. arXiv:1112.4509.
- [99] G. Chachamis, M. Hentschinski, J. D. Madrigal Martinez, A. Sabio Vera, Nucl. Phys. B861 (2012) 133–144. doi:10.1016/j.nuclphysb.2012.03.015. arXiv:1202.0649.
- [100] L. N. Lipatov, Nucl. Phys. B452 (1995) 369–400. doi:10.1016/0550-3213(95)00390-E. arXiv:hep-ph/9502308.

- [101] L. N. Lipatov, *Phys. Rept.* 286 (1997) 131–198. doi:10.1016/S0370-1573(96)00045-2. arXiv:hep-ph/9610276.
- [102] A. V. Lipatov, M. A. Malyshev (2016). arXiv:1606.02696.
- [103] A. D. Martin, M. G. Ryskin, G. Watt, *Eur. Phys. J. C* 66 (2010) 163–172. doi:10.1140/epjc/s10052-010-1242-5. arXiv:0909.5529.
- [104] K. A. Olive, et al. (Particle Data Group), *Chin. Phys. C* 38 (2014) 090001. doi:10.1088/1674-1137/38/9/090001.